Speleothem evidence for C3 dominated vegetation during the Late Miocene (Messinian) of South Africa

Philip J. Hopley, Hazel Reade, Randall Parrish, Michiel De Kock, Justin W. Adams

PII: S0034-6667(18)30158-1
DOI: https://doi.org/10.1016/j.revpalbo.2019.02.006
Reference: PALBO 4054

To appear in: *Review of Palaeobotany and Palynology*

Received date: 11 July 2018
Revised date: 15 February 2019
Accepted date: 16 February 2019

Please cite this article as: P.J. Hopley, H. Reade, R. Parrish, et al., Speleothem evidence for C3 dominated vegetation during the Late Miocene (Messinian) of South Africa, Review of Palaeobotany and Palynology, https://doi.org/10.1016/j.revpalbo.2019.02.006

Speleothem evidence for C_3 dominated vegetation during the Late Miocene (Messinian) of South Africa

Philip J. Hopley[1,2], Hazel Reade[3], Randall Parrish[4,5], Michiel De Kock[6], Justin W. Adams[7,8]

1. Department of Earth and Planetary Sciences, Birkbeck College, University of London, London, UK.

2. Department of Earth Sciences, University College London, London, UK.

3. Institute of Archaeology, University College London, London, UK.

4. School of Earth and Environmental Sciences, University of Portsmouth, Portsmouth, UK

5. NERC Isotope Geosciences Laboratories, British Geological Survey, Keyworth, Nottingham, UK.

6. Department of Geology, University of Johannesburg, South Africa.

7. Centre for Human Anatomy Education, Department of Anatomy and Developmental Biology, Monash University, Melbourne, Australia.

8. Centre for Anthropological Research, University of Johannesburg, South Africa.

Abstract

During the Late Miocene, Africa experienced a number of ecological transitions including the spread of C_4 grasslands, the expansion of the Sahara Desert, the Messinian Salinity Crisis and a number of mammalian migrations and expansions, including the origin of the hominin clade. A detailed understanding of the relationship between environmental change and hominin evolution is hampered by the paucity of data available from terrestrial localities, especially in southern Africa. Here, we present a stable isotope and trace element record from a speleothem from the South African cave site of Hoogland. Uranium-lead dating and magnetostratigraphy places the speleothem within the Messinian Age (7.25 Ma – 5.33 Ma) of the Late Miocene, making it the oldest known cave deposit from the region near the UNESCO Fossil Hominids of South Africa World Heritage Site (locally known as the 'Cradle of Humankind'). Low carbon isotope values indicate a predominantly C_3 vegetation in the vicinity of the cave throughout the period of speleothem growth. It is not possible to determine if this represents a C_3 grassland or a C_3 woodland, but it is clear that an equivalent C_3 –rich environment has yet to be found during the Messinian of east Africa. We conclude that the C_4 grass expansion occurred millions of years later in South Africa than it did in eastern Africa, and that this vegetation shift should be considered when comparing African vegetation change with the late Miocene hominin fossil record.

Keywords: Messinian; speleothem; U-Pb age; stable isotopes; C_3 vegetation; South Africa

Introduction

The Late Miocene represents an important period in African climate history because of its association with the expansion of C_4 grasslands. Since the Oligocene, the trend towards a cooler, drier climate has intensified (Zachos et al. 2001), perhaps in response to the uplift of the Tibetan Plateau (Dupont-Nivet et al., 2008) and subsequence atmospheric CO_2 drawdown (Garzione, 2008). Molecular evidence for the divergence times of C_4 grass lineages in Africa, and globally (Christin et al., 2008), coincide with the reduction in atmospheric CO_2 during the early Oligocene (Zhang et al., 2013), as predicted by the quantum yield predictions of Ehleringer et al. (1997). However, geological evidence for the expansion of C_4 savannah grasslands does not occur until the Middle to Late Miocene (Cerling et al., 1997; Segalen et al., 2007) when further reductions in atmospheric CO_2 were modest, or absent (Pagani et al., 1999; Kürschner et al., 2008). Possible explanations for this expansion of C_4 grasses across Africa include increasing seasonal aridity and/or the increasing role of fire in savannah ecosystems (Osborne, 2007; Scheiter et al., 2012). In addition to C_4 grass expansion, the Latest Miocene was a time of North African (Colin et al., 2014), and possibly global (Ivanovic et al., 2014), climatic change due to the repeated closure and evaporation of the Mediterranean Sea between 5.9 Ma and 5.33 Ma, known as the Messinian Salinity Crisis (Flecker et al., 2015). In addition to these global changes were regional and local environmental modifications associated with tectonic events such as east African uplift (Sepulchre et al., 2006) and closure of the Tethys Ocean (Zhang et al., 2014).

The late Miocene expansion of savannah (C_4) grasslands across Africa (Cerling et al., 1997; Segalen et al., 2007) has been tentatively tied to events within mammalian and hominin evolution (Hopley et al., 2007b; Cerling et al., 2011; Dominguez-Rodrigo, 2014). This is because the earliest putative fossil hominin remains are found in the Late Miocene of Africa; the 6 Ma to 7 Ma *Sahelanthropus tchadensis* from Chad (Brunet et al., 2002; Brunet et al., 2005; Lebatard et al., 2008), the 6.2 Ma to 5.8 Ma *Orrorin tugenensis* from Kenya (Pickford and Senut, 2001; Senut et al., 2001), and the 5.8 Ma to 5.2 Ma *Ardipithecus kadabba* from Ethiopia (Renne et al., 1999; Haile-Selassie, 2001; Haile-Selassie et al., 2004), see Figure 1. Carbon isotope evidence from fossil herbivores and palaeosols associated with these hominins indicates that C_4 grasses were a significant part of the local flora during this earliest phase of human evolution (Boisserie et al., 2005; Levin, 2013; Roche et al., 2013; Simpson et al., 2015). The current estimate for the age of the last common ancestor (LCA) of chimpanzees and humans is at least 7-8 Ma (Langergraber et al., 2012), which post-dates the first occurrence of C_4 grasses in eastern Africa during the Mid-Miocene (Morgan et al., 1994; Cerling et al., 1997) by millions of years. This

apparent lack of temporal overlap between savannah grassland expansion and the evolution of hominin bipedalism has made the intuitively plausible Savannah Hypothesis of human origins a less tenable, and highly debated, proposition (White et al., 2009; Cerling et al., 2010; Roche et al., 2013; Dominguez-Rodrigo, 2014).

Debate about the role of savannah expansion in hominin evolution has tended to focus, with good reason, on eastern Africa (White et al., 2009; Cerling et al., 2010). This is because eastern Africa has a largely continuous record of hominin fossil finds from 6.2 Ma onwards (Pickford and Senut, 2001; Senut et al., 2001), and a co-occurring proxy record of woody cover, derived from east African palaeosol $\delta^{13}C$ values (Cerling et al., 2011). A large sample of hominin fossils has also been collected from South African caves, but due to the vagaries of karstic processes, they have a rather restricted temporal range – currently about 3.5 Ma to Late Pleistocene (Berger et al., 2010, 2015; Granger et al., 2015; Dirks et al., 2017; Hopley et al., in press). There are no known vertebrate fossil assemblages older than 4 Ma from the summer rainfall region of southern Africa, and therefore no hominin fossils from the 7 Ma to 4 Ma time range. This lack of fossil-bearing deposits cannot be used to infer an absence of southern African hominins at this time; it is therefore possible that the biogeographic range of the earliest hominins extended into southern Africa, as it did during later periods. Although the palaeoclimate record of southern Africa is also sparse, with discontinuous or low-resolution data coming from speleothems (Hopley et al., 2007a,b), fossil herbivores (Lee-Thorp et al., 2007) or ratite eggshell (Segalen et al., 2006), there is mounting evidence for a distinct pattern of origin and expansion of the C_4 grasses in this region (Hopley et al., 2007a; Segalen et al., 2007, Lüdecke et al., 2016).

Evidence from sediment cores off the west coast of Namibia and South Africa (Dupont et al., 2013; Hoetzel et al., 2013; 2015) show that C_4 vegetation was not a significant part of the ecosystem until about 6 Ma (see Figure 1). Ocean cores provide long records of climate and vegetation change, but they represent a mean vegetation signal sampled across vast river catchments and have a low temporal resolution (currently about 100,000 years between data-points). Given the ample evidence for topographic vegetation gradients (Reynolds et al., 2011) and shifting vegetation regimes across orbital cycles (e.g. Kingston, 2007; Hopley and Maslin, 2010), it is currently difficult to assess the extent to which different plant functional types were present during the broad timespan of the Late Miocene of southern Africa. Speleothems offer an additional approach to palaeoclimate reconstruction, as they are both high-resolution (between annual and decadal resolution) and carbon isotope measurements can represent the local palaeovegetation structure within the vicinity of the cave (e.g. Hopley et al., 2007a; Holzkamper et al., 2009). Here we undertake a stable isotope study of a Late Miocene speleothem from Hoogland (see Figure 2), a South African palaeocave within the established

protected buffer zone to the east of the UNESCO Fossil Hominids of South Africa World Heritage Site (also referred to as the 'Cradle of Humankind').

The Hoogland Palaeocave

This study centers upon the Hoogland karstic system (25°48'48.30" S, 28° 0'20.40" E), in the Schurveberg Mountain area (the eastern part of the Magaliesberg range), Gauteng Province, South Africa (Figure 2). The Hoogland locality is located ~20 km west of Pretoria within the eastern part of the protected buffer zone of the 'Cradle of Humankind' and is located within the dolomitic terrain of the Malmani Subgroup, which formed as part of the Transvaal Supergroup during the Late Archaean – Early Proterozoic (Eriksson and Altermann, 1998). The modern topography of the area immediately surrounding Hoogland exhibits moderate relief defined by a series of hills and valleys (reaching ~1500 m a.s.l.). Hoogland lies within the catchment of one of the northern meanders of the Hennops River, such that the river is 0.75 km to the east, 1.4 km to the west, and 1.75 km to the north of the karstic system. The Hoogland palaeocave rests at 1494 m a.s.l. on the southern face of a 1540 m a.s.l. hill that courses northwest-southeast within the meander. To the south and east of the locality there is a relatively flat ~600 m^2 floodplain at an altitude of 1425 m a.s.l. As a consequence, Hoogland – like the high-relief localities of Haasgat and Gondolin - show distinct fossil assemblages and taphonomic processes in comparison with the nearby low relief sites of the Blauubank Stream Valley, such as Sterkfontein, Swartkrans and Kromdraai (Adams et al., 2007, Herries et al., 2006a; Adams, 2010, 2012; Herries and Adams, 2013; Leece et al., 2016; Adams and Rovinsky, 2018; Adams, 2018).

Hoogland, similar to the many other karstic sites in the region, was extensively mined in the early 20th century, leaving behind a large volume of *ex situ* breccia dumps, as well as *in situ* deposits along the margins of the original deposit. This opencast speleothem mining obliterated most of the sediment-filled vertical shafts that would have intersected the hillside above the Hoogland site and connected with the original entrance to the karstic system at a higher elevation than the modern remnants. Given the different erosion rates of dolomite between hilltops and valley floors (potentially as disparate as 4m/Myr for hilltops and 52m/Myr for valley floors; Dirks et al., 2010), the morphology and hydrology of the original Hoogland cave system cannot be firmly established (as is the case at other Cradle of Humankind palaeocave systems).

The faunal assemblage currently described from Hoogland is derived from the sampling of nine densely fossiliferous (Number of Identified Specimens, NISP: 4,327) *ex situ* sediment blocks that correspond to the FBU (Flowstone Bounded Unit) 5 *in situ* deposits (Adams et al., 2010). Unlike other regional assemblages, the Hoogland *ex situ* sample is primarily comprised of small skeletal elements and isolated teeth, and as a result these few blocks have yielded a large number of individuals

(Minimum Number of Individuals, MNI: 76) from a wide taxonomic range of vertebrates (e.g., three Classes and six mammalian Orders represented) (Adams et al., 2010). This suggests that the sampled blocks, and at least part of the correlated FBU 5 *in situ* deposits, represent a size-filtered aggregation that formed after primary comminution of skeletal materials and subsequent winnowing within the karstic environment.

Site Chronology

The Hoogland palaeocave entrance was once a near vertical circular shaft, under which a talus cone of external material accumulated. This material was subsequently washed down into a lateral cavern that extended back into the current hillside. At the base of the Hoogland sequence is a ~2m thick sequence of speleothems and siltstones (the 'Basal Speleothem'; Adams et al., 2010), the focus of this study, which is overlain by laminations of siltstone and gravel, representing periodic flooding events that washed material down from the talus cone. This overlying siltstone and gravel deposit is divided into separate accumulation units by flowstone layers ('Flowstone Bounded Units' (FBUs), as at Gladysvale (Pickering et al., 2007) and Buffalo Cave (Herries et al., 2006b)). Of these FBUs, it is 4, 5, and 6 that display dense fossil accumulation. Preliminary palaeomagnetic analysis (Adams et al., 2010), combined with interpretation of the faunal record, suggests the upper deposits of FBU 4-6 fall within the Gauss normal polarity period (3.03 - 2.58 Ma).

Methods

A continuous 1.2 m long sequence of the Hoogland Southern Basal Speleothem, consisting of individual overlapping sections, was collected in May 2009 (Figure 3). Each speleothem section was cut perpendicular to the growth axis, and polished for visual assessment. Powder samples, taken at 30mm intervals using a 2mm-diameter diamond-tipped drill bit, were analysed for calcite/aragonite content by x-ray diffraction (XRD), using a Philips PW 1710 powder diffractometer with PC-APD, at Birkbeck College, University of London. Analysis was conducted using Copper K alpha radiation at 40 kV and 30 mA, with a scan range of 25° to 31° at 2θ. Samples were prepared using distilled water and allowed to air-dry on glass slides. While this method produces some sample orientation it only requires a small volume of material for analysis (Cheetham, 2002). Six thin sections were produced from representative samples; speleothem fabrics were identified using previously published speleothem studies (Frisia et al., 2000, Frisia et al., 2002, Hopley et al., 2009, Frisia, 2015). Block samples for palaeomagnetic analysis were oriented in the field using a Suunto Compass and Clinometer. Palaeomagnetic analyses of the speleothem were completed using a 2G-Enterprises™ superconducting rock magnetometer with an automatic sample changer (Kirschvink et al., 2008)

housed at the University of Johannesburg. Each sample was demagnetized in approximately thirteen demagnetization steps. Steps included a measurement of natural remanent magnetization (NRM), alternating-field (AF) cleaning in four 2.5 mT steps up to 10 mT, and thermal demagnetizion steps from 100°C to 525°C. Thermal demagnetization was completed within about 8 decreasing increments, or until specimen intensity dropped below instrument noise level (below ~8 x 10^{-8} Am2). Magnetic components were identified and quantified via least squares analysis (Kirschvink, 1980) utilizing Paleomag 3.1 (Jones, 2002).

Sampling for stable isotope and trace element analysis was conducted at 5mm intervals, using a 2mm diameter diamond-tipped drill bit, down to a depth of 640 mm from the top of the speleothem. Below 640 mm sampling resolution was reduced to 30 mm intervals; in total 182 powdered samples were drilled. Isotopic analysis took place at the Bloomsbury Environmental Isotope Facility (BEIF), University College London, on a gas-source mass spectrometer. Analysis was conducted on samples of ~0.4 mg. Errors ranged from 0.03 ‰ - 0.05 ‰ and 0.18 ‰ - 0.34 ‰ at 1 standard deviation for $\delta^{13}C$ and $\delta^{18}O$ respectively. Trace element analysis required ~10 mg of powder to be dissolved in 4 ml of 10% HCl. Samples were analysed in the Wolfson Laboratory for Environmental Geochemistry, University College London, on a Horiba JY Ultima 2C ICP-AES.

Initial *in situ* measurements of $^{207}Pb/^{206}Pb$ and $^{238}U/^{206}Pb$ ratios were made using Laser Ablation (LA) ICP-MS at the NERC Isotope Geoscience Laboratory (NIGL). The accuracy of these ratios was assured through the use of a calibrated solid calcite reference material of known and measured age and isotope composition (Roberts et al., 2017). A New Wave 193 nm solid state laser ablated the polished sample surface, previously loaded into the ablation cell. The LA pit produced is usually 30µm in diameter, and approximately 10 µm deep, taking about 1 minute per analysis. The mass spectrometer used was the NuPlasma HR ICP-MC-MS equipped with multiple detectors. Other isotopes were also measured (204 mass of Pb and Hg, ^{201}Hg, ^{235}U-^{205}Tl solution) to assist with data reduction and correction for signal stability. Corrections for detector gains and other parameters, mass discrimination of Pb, and inter-element normalisation was done through the measurement of the WC-1 calcite standard of known age (254 Ma; Roberts et al. 2017; Table S5 and Figure S1), a mixed solution of ^{235}U and ^{205}Tl, and a NIST glass containing Pb of known isotope composition. The uncertainty on the measured age of the calcite standard is ±2-3% at the 95% confidence level for $^{238}U/^{206}Pb$ ratios. Any further uncertainty associated with standard reproducibility was quadratically added to this value, taking into account the performance on the day of measurement.

Following promising initial measurements by LA-ICP-MS, the age was verified by sub-sampling relevant parts of the sample, dissolving these materials in the addition of an isotope tracer, chemically

separating the U from Pb and purifying these elements on ion exchange resins, followed by high precision measurement of U and Pb isotope composition by TIMS methods (thermal ionisation mass spectrometry) at NIGL. This method does not rely on a mineral standard and has inherently higher measurement accuracy and precision than the laser ablation method, revealing modest heterogeneity in the sample not apparent with LA-ICP-MS. This approach has the added advantage that the ^{204}Pb can be accurately measured and the data can be plotted on both Tera-Wasserburg and normal isochron diagrams, allowing a determination of the initial ^{206}Pb/^{204}Pb and ^{207}Pb/^{204}Pb and ^{207}Pb/^{206}Pb values. In addition, it is possible to plot a ^{235}U-^{207}Pb-^{204}Pb isochron as well, though this is less precise.

Finally, the uranium activity ratio must be measured at the highest precision possible. It has been demonstrated that the initial activity ratio of uranium ^{234}U/^{238}U ratio within a speleothem can differ significantly from the secular equilibrium value of 1.0. The activity ratio is designated as [U]i where i refers to the initial value, as opposed to the present day measured value. A value of [U]i > 1.0 means there was excess ^{234}U in the water which when incorporated into calcite will decay into ^{206}Pb, raising the measured ^{206}Pb/^{238}U ratio and age by an amount related to the activity excess above 1.0. It is only possible to determine the initial [U], and therefore make a correction for the excess age, if the precisely measured value of [U] is different than 1.0. This requires for older samples a very high precision measurement of the U isotope composition in a sample. This was done by sampling the material in duplicate, dissolving it, separating and purifying the U from the calcite using ion-exchange columns, and determining its precise U isotope composition using a Thermo Neptune ICP-MC-MS at NIGL. The correction for initial excess [U] was calculated using an in-house Excel programme, based on the iterative methods described by Wendt and Carl (1985). This calculation assumes that the initial ^{230}Th activity is zero, i.e. the water that deposited the speleothem was devoid of Th, while being enriched in U. The ^{235}U-^{207}Pb decay system does not suffer from such an acute issue with initial excess ^{234}U activity, because no intermediate daughter isotope in the decay chain is composed of uranium; instead it is ^{231}Pa which is thought to have very low solubility in water, and would therefore not lead to any substantial excess age. Therefore, the ^{235}U-^{207}Pb age cited should be free from the significant age uncertainty arising from the initial disequilibrium of daughter isotopes in the drip waters.

Results

Petrography Results

The Hoogland Southern Basal Speleothem displays a broad range of speleothem fabrics, indicative of changing depositional environments through time (Figure 4). In the top 620 mm the fabric varied between opaque microcrystalline calcite, light-brown horizontally laminated flowstone composed of

columnar calcite crystals, and curved calcite crystallites belonging to the lattice deformation fabric (Figure 5a,b), as described by Broughton (1983). The lattice deformation fabric occurs due to calcite growth on curved surfaces such as stalactites (Broughton, 1983) and mammillary speleothems (Hopley et al., 2009); mammillary speleothems are common in palaeokarst sequences from the Cradle of Humankind, including Hoogland (Adams et al., 2010), and typically form in subaqueous (e.g. cave pool) environments (Hill and Forti, 1997; Polyak et al., 2008). Below a depth of 620 mm, thick layers of needle aragonite (Figures 4, 5e,f) and highly porous 'vuggy' textures dominate. XRD analysis reveals that the Hoogland basal speleothem is composed primarily of calcite, but with a notable proportion of aragonite. Pure calcite is present at depths of 60 – 120 mm, 390 – 450 mm and below 960 mm. Minor aragonite occurs in samples at the very top of the sequence and at depths of 150 – 300 mm, and 870 – 930 mm. The proportion of aragonite significantly increases below 480mm depth, which corresponds with the observations made from visual assessment. The presence of minor amounts of aragonite indicates that the majority of calcite identified is most likely of secondary formation. The layers identified as pure calcite by XRD analysis show lattice-deformed mammillary and columnar (radiaxial fibrous) calcite (Figure 5c) fabrics (Broughton, 1983; Frisia, 2015). This lattice deformed mammillary calcite can clearly be seen in the low magnification thin sections, for example at the top of thin section 1 in Figure 4. The mosaic calcite crystals of Figure 5d and 5f are typical of diagenetic (secondary) calcite (Folk and Assereto, 1976; Frisia, 2015) and correspond to XRD samples identified as calcite with a minor aragonite component. Large primary aragonite needle crystals (Figure 5e) are present at depths corresponding to XRD samples identified as containing significant proportions of both calcite and aragonite. Figure 5f displays both large primary aragonite crystals and secondary mosaic calcite, providing evidence for the diagenetic transformation of aragonite to calcite. The primary columnar calcite fabric (Figure 5c) is similar to that described as radiaxial fibrous by Frisia (2015), and is indicative of sub-aerial deposition; as shown in Figure 4, this fabric is rare within the Hoogland speleothem.

Stable isotope results

Stable isotope values were produced for 174 sub-samples from the Hoogland Southern Basal Speleothem (see Supplementary Table S1). $\delta^{18}O$ values ranging from -6.35 ‰ to -3.63 ‰ (mean = -5.11 ± 0.37 ‰), with $\delta^{13}C$ values ranging from -10.18 ‰ to -4.26 ‰ (mean = -8.09 ± 1.36 ‰). No significant trend in the $\delta^{18}O$ data is present (Figure 6). $\delta^{13}C$ results display a significantly higher variability and fall within the range of expected values for both a C_3 vegetation and a mixed C_3 and C_4 vegetation (McDermott, 2004). Low $\delta^{13}C$ (mean = -9.26 ± 0.59 ‰) values dominate the sequence

between a depth of 400mm and 610mm. $\delta^{13}C$ values > -7.0‰ occur only at depths above 280 mm (mean = -6.62 ± 0.99 ‰). The lack of co-variation (Figure 6) between $\delta^{18}O$ and $\delta^{13}C$ indicates that there is no strong climatic or depositional (e.g. kinetic fractionation) evidence for covariance preserved within the data.

Trace Element Results

Magnesium content (expressed as 1000Mg/Ca) varied from 0.13 to 47.0, while the 1000Sr/Ca ratio varied from 0.01 to 2.29 (Supplementary Table S1, Figure 6). 1000Mg/Ca and 1000Sr/Ca values show a weak negative correlation ($r = -0.31$, $p < 0.001$). The high variability in Mg and Sr content is associated with the different mineral phases (aragonite and calcite) present in the Hoogland Basal Speleothem, as predicted by the different partition coefficients of Mg and Sr into the different minerals (Huang and Fairchild, 2001). The Mg/Ca ratio in the cave water is the primary control on aragonite precipitation, so as predicted, results show a strong relationship between mineral type and Mg/Ca ratio (Figure 6). Less clear, but still apparent, is an inverse relationship between Sr/Ca ratios and speleothem fabric (Figure 6). The values for secondary calcite display intermediate ratios, between the aragonite and primary calcite values. Hopley et al. (2009) interpret similar secondary calcite values as representing the degree of openness of the diagenetic environment, and/or a mixing of the calcite-aragonite end members.

U-Pb dating results

The Hoog X4 laser ablation dataset (see Supplementary Table S2) consists of a linear data array containing a wide spread of data (n = 89), including a number of measurements with low (highly radiogenic) values of $^{207}Pb/^{206}Pb$ and high values of $^{238}U/^{206}Pb$, with the excess scatter in the measurements being small or minimal, i.e. the Mean Square Weighted Deviation (MSWD) of the array is 1.7. This laser ablation dataset produces a U-Pb age of 5.66 ± 0.17 Ma (see Figure 7a). The isotope dilution data set (ID-TIMS) for Hoog X4 (Supplementary Table S4) produces an isochron (n = 5) with an age of 5.390 ± 0.074 Ma on the ^{238}U-^{206}Pb T-W plot (see figure 7b). This is very close to within-error agreement with the laser ablation age, indicating a late Messinian (~5.45 Ma) age determination assuming no initial disequilibrium for this sample. The isotope dilution dataset for the $^{235}U/^{207}Pb$ system produces an isochron age of 4.9 ± 1.9 Ma (see Figure 7d). This age has a high associated error due to scatter and unfortunately cannot be used to refine the age estimates derived from the $^{238}U/^{206}Pb$ system.

The two [U] measurements for Hoog X4 were 0.9987 ± 0.0015 and 0.9967 ± 0.0015; the mean value of 0.9977 ± 0.0014 is marginally different from secular equilibrium (see Supplementary Table S3a). If the [U] measurements are considered to be free from post-depositional alteration, then correction of the $^{238}U/^{206}Pb$ age may be appropriate. If a correction is applied to the mean $^{238}U/^{206}Pb$ age, then the final corrected age would increase by about 0.4 Ma to ~5.8 Ma; in this instance, the initial [U] would be <0.1 (see Supplementary Table S3b), which we consider to be an unrealistically low value. One way to reconcile these measurements is to accept the possibility of a very minor relatively recent modification to the speleothem via addition of a small amount of calcite with [U]<1, or via a minor loss of ^{234}U through leaching. Given the presence of primary and secondary speleothem fabrics within the Hoogland Southern Basal Speleothem (Figures 4 and 5), this is a reasonable assertion.

Reliable correction of Mio-Pliocene U-Pb ages is dependent on accurate and precise [U] measurements in samples that are very close to secular equilibrium, and/or a knowledge of initial $^{234}U/^{238}U$ ratios in speleothems from the studied region. To investigate the likely initial $^{234}U/^{238}U$ ratio of Hoogland X4 we follow the approach taken for other Mio-Pliocene age speleothems (e.g. Polyak et al., 2008; Woodhead et al., 2019) by compiling a list of initial $^{234}U/^{238}U$ ratios for U-Th dated speleothems from the Cradle of Humankind (see Supplementary Table S6). The values range from 1.26 to 2.99 with a mean of 1.9 (s.d. = 0.8, n = 27). These are significantly lower than the values (mean 4.56, s.d. = 3.5, n = 27) for the spring, well and cave waters of northern South Africa reported by Kronfeld et al. (1994). High initial $^{234}U/^{238}U$ values of 5.56 to 6.19 (mean = 5.9, n = 16) do occur in U-Th dated South African speleothems from the Makapansgat Valley and from Wolkberg Cave (Hopley et al., 2018; Holzkamper et al., 2009), but these sites are located approximately 300 km north east of the Cradle of Humankind where the bedrock and hydrological conditions are different. Using the Cradle of Humankind values (Supplementary Table S6), we calculate an initial $^{234}U/^{238}U$ ratio of 1.9 ± 0.8 for a 5.39 Ma speleothem would result in a present day $^{234}U/^{238}U$ value of ~1.0001; a low initial value of 1.3 ± 0.3 would result in a measured value of ~1.00007 (see Supplementary Table S3b). Such values cannot be distinguished from equilibrium, given current analytical precision. Based on our ID-TIMS U-Pb age of 5.390 ± 0.074 Ma (Figure 7b), which is younger and more precise than the LA U-Pb age of 5.66 ± 0.17 Ma (Figure 7a), corrected ages using both of the assumed Cradle of Humankind initial $^{234}U/^{238}U$ ratios (see Supplementary Table S3b) are consistent with a late Messinian age. Our preferred corrected age is 5.28 ± 0.12 Ma, although we acknowledge the possibility of an expanded age range spanning from 5.8 Ma to 4.8 Ma (see Figure 9).

Magnetostratigraphy

Palaeomagnetic analyses of a thin reddish siltsone immediately overlying Hoogland X4 (see Figures 3 and 4) indicates that the top of the Southern Basal Speleothem (SBS) sequence was formed during a reversed polarity. The three repeat analyses of this silty layer dispayed NRMs that were south westerly and upward directed, but during demagnetization a more stable south westerly downward magnetization was revealed (Figure 5a). Weaker magnetized samples of the much cleaner (i.e., silt free) speleothems from lower in the SBS sequence were also dominantly formed during a reversed polarity. Demagnetization proceeded in most cases along trajectories from a south westerly upward direction towards a south westerly downward position (Figure 8b), but in some instances the magnetization of samples dropped below the noise level of the instrument before this position was reached (Figure 8c). Two samples (i.e., PM4 and PM7) were dominated by north easterly upward magnetizations (Figure 8d), which were roughly antipodal to the rest of the samples.

As discussed above, the corrected U-Pb age for Hoogland X4 places the uppermost layers of the Southern Basal Speleothem between 5.8 Ma and 4.8 Ma – most of this time window is within the reversed polarity C3r Gilbert Chron (6.033 – 5.235 Ma; Ogg, 2012); the very youngest part of this age range is within the C3n.3r Gilbert Chron (4.896 – 4.997 Ma; Ogg, 2012). Our paleomagnetic results confirm that the SBS formed during a period of predominantly reversed polarity, which we assign to the C3r Gilbert Chron (Figure 9). Only the lowermost parts of the Southern Basal Speleothem possibly formed during the C3An.1n normal polarity (6.033 – 6.252 Ma; Ogg, 2012), but this is based on the results of a single sample and is thus treated with appropriate caution. With the current dating evidence it is not possible to determine the duration of speleothem growth or to determine whether the observed changes in speleothem fabric (Figure 4) are associated with brief hiatuses.

Discussion

Mineralogical influences on stable isotope values

The predominantly sub-aqueous nature of mineral precipitation combined with the high proportions of metastable aragonite and secondary calcite suggests that the geochemical signals contained within the speleothem are unlikely to reflect a pristine palaeoenvironmental signal. However, the extent to which the measured stable isotope values reflect the carbon and oxygen composition of the cave water can be evaluated. If the isotopic signal had been influenced by the type of mineral precipitating, a correlation between mineral type and $\delta^{18}O$ or $\delta^{13}C$ values can be expected. Results from Hoogland show no clear relationship between mineral type and isotopic values (Figure 6), indicating that

mineralogical differences in isotopic equilibrium/disequilibrium conditions and/or the extent of diagenesis were small. Rapid degassing or evaporation (processes associated with disequilibrium) result in enriched, and positively correlated $\delta^{18}O$ and $\delta^{13}C$ values (Mickler et al., 2006). However, the findings of this study show low, or average $\delta^{18}O$ and $\delta^{13}C$ values (when compared to similar studies e.g. Hopley et al., 2007a, Holmgren et al., 2003), with no positive correlation (Figure 6). In particular, the enriched $\delta^{13}C$ values characteristic of aragonite formation (Romanek et al., 1992) are absent. The widespread evidence for diagenetic processes indicates that even if primary precipitation occurred in isotopic equilibrium, secondary mineral precipitation was extensive enough to disrupt such signals (by enriching values, particularly $\delta^{13}C$ and Mg/Ca and Sr/Ca). However, once again no link between secondary calcite and isotopic enrichment is apparent. This again supports the interpretation that the stable isotopic signals have the potential to represent external influences.

Mg/Ca concentrations predominantly vary according to bedrock dissolution rates and water residence time (Fairchild and Treble, 2009). Comparison with $\delta^{18}O$ values can therefore demonstrate a link with palaeohydrological changes (particularly water influx rates). The changes to water influx rates can either dilute or concentrate Mg/Ca concentrations in the host water, which in turn can influence the precipitation of aragonite over calcite. Mg/Ca (and Sr/Ca) concentrations from Hoogland do not co-vary with $\delta^{18}O$ values (Figure 6). However, it is unclear whether this is owing to the lack of relationship between the two variables, or the possible post-depositional alteration of the of $\delta^{18}O$ signal. Sr/Ca increases below 500mm depth, and Sr is known to be incorporated in larger quantities at higher growth rates (Fairchild and Treble, 2009). Studies have also shown Sr can be used as a proxy for aeolian dust input (e.g. Goede et al., 1998), however this scenario is unlikely for the deep-cave locality of the Hoogland basal speleothem. It is most plausible that the elevated Sr/Ca ratios at the base of the sequence reflect periods of higher growth rates as they correspond with sections of large aragonite ray crystals.

While $\delta^{18}O$ values vary by a similar range to that reported by Hopley et al (2007a) for other Miocene to Pleistocene speleothems from South Africa, the lack of a clear trend or cycle in the depth-series suggests the signal may have been dampened by disequilibrium and/or post-depositional processes. It is also possible that diagenesis could have altered the $\delta^{18}O$ to a greater extent than the $\delta^{13}C$ signal. Therefore, we do not attempt to infer the $\delta^{18}O$ values of Messinian rainfall or to correlate the Hoogland oxygen isotope record with the global benthic $\delta^{18}O$ stack of Zachos et al. (2001, see Figure 1).

Duration of Speleothem Growth

Speleothems typically grow at a rate of between 0.01 mm and 1 mm per year (Baker and Smart, 1995; Genty et al. 2001). The time periods represented by the Hoogland Southern Basal Speleothem, excluding hiatuses, could therefore represent between 1200 years and 120,000 years. A time span at the lower end of this estimate (i.e. faster accumulation rate) is suggested by the predominance of subaqueous speleothem fabrics, combined with the presence of fast growing fans of aragonite rays in some parts of the sequence. Given the variety of crystal structures found within the Southern Basal Speleothem we suggest that growth rate could have varied significantly over time. A lack of knowledge of the relationships between different crystal types and growth rates prevents further interpretation. No clear hiatus events were present in sections sampled. The presence of fine layers of detrital and organic material at various depths could indicate hiatuses in speleothem formation, but could also equally represent higher growth rates, where sediment influx was accelerated, some of which being incorporated in the deposit during mineral precipitation. As speleothem $\delta^{18}O$ and $\delta^{13}C$ can vary with precessionally-forced variations in rainfall in sub-tropical regions such as South Africa, it is often a useful chronological tool (Cruz et al., 2005; Hopley et al., 2007b; Lachniet, 2009). However, the lack of a significant cyclicity in the Hoogland $\delta^{18}O$ and $\delta^{13}C$ depth series prevents further refinement of the chronology using cyclostratigraphy.

Age of the Hoogland speleothem

The palaeocave deposits of the Cradle of Humankind that have been identified and studied are typically considered to be Late Pliocene to Early Pleistocene in age on the basis of biostratigraphic, magnetostratigraphic, and increasingly, radiometric ages (McKee et al., 1995; Walker et al., 2006; Herries et al., 2009; Pickering et al., 2011). The concentration of cave sediments and faunal assemblages within this relatively brief time window has been explained by river incision into the post-Cretaceous African erosion surface due to post-Pliocene uplift associated with the African superswell (Sepulchre et al., 2006; Partridge 2010; Dirks and Berger, 2013). According to this model, the caves would have formed in the phreatic zone when the Paleoproterozoic dolomites were largely covered by the impermeable duricrusts of the African erosion surface (Dirks and Berger, 2013). At approximately 4 Ma, lowering of the water-table and surface erosion drained the caves, and enabled speleothems to form in subaerial and shallow cave pool environments. As exhumation of the caves continued and entrances expanded, surface sediments and faunal remains made their way into the caves (Brain, 1981; Dirks and Berger, 2013). This model of surface erosion and cave development in the Cradle of Humankind is based on existing evidence for cave sediments and speleothems accumulating from the Pliocene onwards.

Previous speleothem U-Pb ages from the Cradle of Humankind have ranged from 2.8 Ma to 1.5 Ma (Walker et al., 2006; Pickering et al., 2011). A cosmogenic isotope age for Sterkfontein Member 2 dates back to the mid-Pliocene at 3.67 Ma ± 0.16 (Granger et al., 2015), although this may be younger than 2.8 Ma given the discordance with published faunal data from the deposit and locality (Reynolds and Kibii, 2011) and if a two-stage burial scenario is considered (Kramers and Dirks, 2017). The oldest purported faunal assemblage in the Cradle of Humankind is from Waypoint 160 on Bolt's Farm which has been assigned an early Pliocene age of approximately 4.5 Ma - 4.0 Ma (Gommery et al., 2014) on the basis of a novel muroid rodent, *Euryotomys bolti*, that is morphologically intermediate between *Euryotomys pelomyoides* (Pocock, 1976) from Langebaanweg E Quarry (5.0 Ma) and the earliest known representatives of the Otomyinae from the Makapansgat Limeworks, dated tentatively to ~3.0 Ma (Denys, 1999; Hopley et al., 2006). As a result, there is effectively no first or last appearance date for *E. bolti* that independently informs on the age of the Waypoint 160 deposits or supports this specific age range. Our reading of the literature indicates that there is currently no secure radiometric or biochronological evidence for cave sediments older than ~3.0 Ma in the Cradle of Humankind. The addition of new U-Pb and magnetostratigraphic evidence from the Hoogland Southern Basal Speleothem (Figures 7 & 8) indicates speleothem growth during the Messinian Salinity Crisis between approximately 6.0 Ma and 5.3 Ma (see Figure 9). This makes the Southern Basal flowstone the oldest dated cave deposit in South Africa, and the first Late Miocene sediments to be identified from the Cradle of Humankind. These Late Miocene cave deposits push back the age for uplift and river incision in this region, and increase the likelihood of discovering Late Miocene cave sediments and faunal assemblages in the Cradle of Humankind. An expanded Late Neogene sedimentary sequence in South Africa provides sediments overlapping in time with hominin-bearing sediments in eastern (Cerling et al., 2011) and northern (Brunet et al., 2002) Africa (as shown in Figure 1).

Carbon Isotope Palaeovegetation Proxy

If the carbon isotope composition of speleothems has been altered by diagenetic processes, or by rapid degassing during initial mineral precipitation, $\delta^{13}C$ values are likely to increase, along with an associated rise in Mg/Ca and Sr/Ca ratios (Mickler et al., 2006; Fairchild and McMillan, 2007). However, unlike other studies on secondary calcite speleothems (e.g. Hopley et al., 2009; Holzkämper et al., 2009), the $\delta^{13}C$ values in the Hoogland Southern Basal Speleothem are low (Figures 6 & 10), significantly below that of the Malmani dolomite host rock. There is also no correlation between $\delta^{13}C$ and Mg/Ca or Sr/Ca ratios. As such, the $\delta^{13}C$ composition of the speleothem does not appear to reflect a large proportion of water-rock interaction, or kinetic fractionation effects, either during primary

aragonite deposition, or during secondary calcite precipitation. This suggests that the $\delta^{13}C$ values can be used as a proxy for palaeovegetation in a similar manner as at other South African cave sites (e.g. Hopley et al., 2007a; Holmgren et al., 2003). Using the method set out in Genty et al., 1999a and 1999b, and assuming soil CO_2 $\delta^{13}C$ values of -25‰ and -11‰ for pure C_3 and C_4 vegetation respectively (Holzkämper et al., 2009) and a bedrock component of 15% (with a $\delta^{13}C$ value of -0.9 ± 0.7‰ (Veizer et al., 1992)), C_3 vegetation would be represented by $\delta^{13}C$ values of around -9‰, while pure C_4 vegetation would have values of around +1‰. The majority of $\delta^{13}C$ values from Hoogland are therefore indicative of a purely C_3 vegetation, particularly at a depth below ~350mm. Above a depth of 350 mm, the $\delta^{13}C$ values show a trend towards higher values, possibly indicating an increased presence of C_4 vegetation (up to 42%, based on the above end-member values). However, with multiple possible causes for increased $\delta^{13}C$ values in these speleothems (e.g. Baker et al., 1997; Hopley et al., 2009), an increased C_4 plant proportion cannot be proposed with a high degree of confidence.

Comparison of the Hoogland $\delta^{13}C$ data with other published records of Miocene to Pleistocene South African speleothems shows that low $\delta^{13}C$ values, indicative of C_3 vegetation, is typical of the older speleothems (see Figure 10). The Hoogland speleothem has a similar mean $\delta^{13}C$ value to that of the Collapsed Cone flowstone from the Makapansgat Valley (Hopley et al., 2007a), but shows far greater isotopic variability; this is most likely due to the mixed mineralogy and range of cave environments represented by the Hoogland speleothem. While the C_3 environment of the Collapsed Cone flowstone is clear, the speleothem is not amenable to U-Pb dating due to very low U content and unfavourable U-Pb ratios; magnetostratigraphic age constraints place the growth of the speleothem to between approximately 4.0 Ma and 5.0 Ma (Hopley et al., 2007a). The late Messinian age of the Hoogland speleothem provides valuable absolute age constraints on the timing of the transition from a C_3 to a C_4 vegetation in South Africa. All younger speleothems from South Africa (2.0 Ma to recent) show a mixed C_3 and C_4 vegetation, typical of the savannah woodland prevalent in the modern day (see Figure 10).

Messinian Vegetation and Climate

Growth of the Hoogland Southern Basal Speleothem sequence occurred during the Messinian Salinity Crisis (MSC), a North African and Mediterranean climatic event dating between 5.97 Ma and 5.33 Ma (Manzi et al., 2013; see Figure 1). The Messinian Salinity Crisis was characterised by the restriction and closure of marine gateways between the Mediterranean Sea and Atlantic Ocean which resulted in extreme salinity fluctuations in the Mediterranean leading to the precipitation of thick evaporate deposits during the late Messinian. It is clear that this event had major impacts on the biogeography

and climate of the Mediterranean / North African region (Flecker et al., 2015), but the extent to which the climate impacts of the MSC extended beyond this region is currently unknown. A modelling sensitivity study by Schneck et al. (2010) indicated that at approximately 1500 m below sea level, the desiccated floor of the Mediterranean basin during the MSC would have been up to 7 °C warmer, and that the temperature of the surrounding region would have changed by up to 2 °C. It is likely that these increased temperatures were accompanied by increased aridity in northern Africa (Otero et al., 2011), and perhaps an increase in C_4 vegetation and an expansion of the Sahara Desert at this time (Zhang et al., 2014). Elsewhere in sub-Saharan Africa, simulated temperature anomalies during the MSC are small and insignificant (Schneck et al., 2010; Bradshaw et al., 2012). Opportunities to validate these Messinian climate simulations with palaeotemperature or palaeovegetation data are limited by the lack of proxy data from the Messinian of Africa, particularly southern Africa (Bradshaw et al., 2012). In this study we are able to provide an initial glimpse of the vegetation of South Africa during the Messinian.

The present study demonstrates that an exclusively C_3 vegetation was at times present during the Messinian Salinity Crisis in South Africa. It is possible that some C_4 vegetation was present during the arid phase of a precessional cycle, however due to compounding factors, this cannot be established with confidence. What this study does show is that a purely C_3 vegetation was present (either continuously, or intermittently across precessional cycles) in the summer rainfall zone of South Africa, millions of years after C_3 dominated vegetation disappeared from the present-day savannahs of eastern and northern Africa (e.g. Cerling et al., 2011). As is the case in other regions of Africa, there is little macrofossil or geochemical evidence for the flora that preceded the spread of C_4 grasslands in South Africa. Given the evidence for closed canopy forest during discreet intervals within the Plio-Pleistocene of South Africa, including extremely low $\delta^{13}C$ values in some fossil herbivore teeth from Haasgat (Adams et al. 2013) and fossil wood from Sterkfontein (Bamford et al., 1999), it seems likely that woodland or forest would have been prevalent during the late Messinian at Hoogland. Forest-dwelling species, including the arboreal hominoid *Otavipithecus namibiensis*, are typical of the Middle to Late Miocene of Namibia (Conroy et al., 1992; Senut et al., 1992; Senut and Gommery, 1997); we envisage a similar woodland/forest environment during the late Messinian of Hoogland.

Previous studies have suggested that the spread of C_4 grasses occurred later in southern Africa than it did in eastern and Northern Africa (Pickford, 2004; Segalen et al., 2007; Dupont et al., 2013; Lüdecke et al., 2016), but poor age-constraints and restricted geological successions have prevented precise chronologies for the origin of C_4 grasses in the southern Africa interior (e.g. Hopley et al., 2007a),

where early hominin discoveries are common (Berger et al., 2010; Berger et al., 2015). Here we demonstrate a post-Messinian spread of C_4 grasses in South Africa, millions of years later than the mid-Miocene (15 Ma) expansion of C_4 plants across equatorial Africa (e.g. Cerling et al., 1997). This delayed expansion of C_4 grasses in to South Africa fits with the quantum yield model of Ehleringer et al. (1997), which predicts a temperature/latitudinal control over C_3/C_4 plant distribution; it is also likely that reduced rainfall (Dupont et al., 2013) and increased occurrence of fire (Hoetzel et al., 2013) played a role in the eventual arrival of C_4 plants in South Africa during the Pliocene. Whether this event had any impact on the evolution of early hominins in South Africa and elsewhere in Africa (e.g. Pickford, 2004) remains an open question.

Conclusion

This study has found that the basal speleothem at Hoogland formed during the late Messinian, at approximately 5.5 Ma, making it the oldest cave deposit from the Cradle of Humankind, and the first evidence of Miocene cave infill in this region. The speleothem is composed of thin layers of calcite interspersed with metastable aragonite, most of which has been diagenetically altered to secondary calcite. The mixed mineralogy of the speleothem impacts the interpretation of the $\delta^{18}O$ values as an indicator of palaeoprecipitation, but the low $\delta^{13}C$ values are a valuable palaeovegetation indicator. The low $\delta^{13}C$ values of the primary calcite indicate an exclusively C_3 vegetation overlying the cave during the late Messinian, and in conjunction with other South African speleothems (Hopley et al., 2007a), indicates a post-Messinian age for the expansion of C_4 vegetation in South Africa. The equivalent expansion of C_4 vegetation in equatorial Africa occurred millions of years earlier (15 Ma – 12 Ma) in the Mid-Miocene (Morgan et al., 1994; Cerling et al., 1997; 2011) indicating distinct vegetation histories in these two hominin-yielding regions. Previous assertions that the African palaeovegetation record fails to support the savannah hypothesis of human origins (White et al., 2009; Dominguez-Rodriguez, 2014) should be reconsidered in the light of a post-Messinian shift in South African vegetation.

Acknowledgements

This project was completed with financial assistance from the Quaternary Research Association (QRA) to H.R. and the Leakey Foundation to P.H. Additional funding from Grand State Valley University (JWA), and the University of Witswatersrand (to J.W.A. and Jason Hemingway), and the National Science Foundation (BCS 0962564) are also acknowledged. This project was kindly supported by the

landowner of the site, Dr Kruger, and the South African Heritage Resource Agency (SAHRA) who granted permits to acquire the samples. Janet Hope, Jim Davy, Tony Osborn (University College London) and Steve Hirons (Birkbeck, University of London) provided technical support during laboratory analysis. Staff at the NERC Isotope Geosciences Laboratory are thanked for their substantial assistance in data collection. We would like to thank José Carrión for his editorial support and the anonymous reviewers for their constructive comments.

References

Adams, J. W., 2010. Taphonomy of the Gondolin GD 2 in situ deposits and its bearing on interpretations of South African Plio-Pleistocene karstic fossil assemblages. *Journal of Taphonomy* 8, 81-116.

Adams, J. W., 2012. A revised listing of fossil mammals from the Haasgat cave system *ex situ* deposits (HGD), South Africa. *Palaeontologia Electronica* 15 (3), 29A, 88p.

Adams, J. W., Hemingway, J., Kegley, A. D. T., Thackeray, J. F., 2007. Luleche, a New Paleontological Site in the Cradle of Humankind, North-West Province, South Africa. *Journal of Human Evolution* 53, 751-754.

Adams, J. W., Herries, A. I. R., Hemingway, J., Kegley, A. D. T., Kgasi, L., Hopley P., Reade H., 2010. Initial fossil discoveries from Hoogland, a new Pliocene primate-bearing karstic system in Gauteng Province, South Africa. *Journal of Human Evolution* 59, 685-691.

Adams, J. W., Kegley, A. D. T., Krigbaum, J., 2013. New faunal stable carbon isotope data from the Haasgat HGD assemblage, South Africa, including the first reported values for *Papio angusticeps* and *Cercopithecoides haasgati*. *Journal of Human Evolution* 64, 693-698.

Leece, A., Kegley, A. D. T., Lacruz, R., Herries, A. I. R., Hemingway, J., Potze, S., Kgasi, L., Adams J. W., 2016. The first reported hominin from Haasgat and the limitations of dental microstructure for the taxonomic attribution of early Pleistocene hominins in South Africa. *PeerJ* 4, e2024.

Adams, J. W, Rovinsky, D. S., 2018. Taphonomic interpretations of the Haasgat HGD assemblage: a case study in the impact of sampling and preparation methods on reconstructing South African karstic assemblage formation. *Quaternary International* 495, 4-18.

Adams, J. W., 2018. Fossil faunas from the Gondolin Dump A *ex situ* hominin deposits, South Africa. *PeerJ* 6, e5393.

Baker, A., E. Ito, P. L. Smart, McEwan, R. F., 1997. Elevated and variable values of C-13 in speleothems in a British cave system. *Chemical Geology* 136, 263-270.

Baker, A., Smart, P. L., 1995. Recent flowstone growth rates: Field measurements in comparison to theoretical predictions. *Chemical Geology* 122, 121-128.

Bamford, M., 1999. Pliocene fossil woods from an early hominid cave deposit, Sterkfontein, South Africa. *S. Afr. J. Sci.* 95, 231-237.

Berger, L. R., Pickering, R., Kuhn, B., Backwell, L., Hancox, P. J., Kramers, J. D. Boshoff, P., 2009. A Mid-Pleistocene *in situ* fossil brown hyaena (*Parahyaena brunnea*) latrine from Gladysvale Cave, South Africa. *Palaeogeography, Palaeoclimatology, Palaeoecology* 279, 131-136.

Berger, L. R., de Ruiter, D. J., Churchill, S. E., Schmid, P., Carlson, K. J., Dirks, P. H. G. M., Kibii, J. M., 2010. *Australopithecus sediba*: A New Species of *Homo*-Like Australopith from South Africa. Science 328, 195-204.

Berger, L. R., Hawks, J., de Ruiter, D. J, Churchill, S. E., Schmid, P., Delezene, L. K., Kivell, T. L., Garvin, H. M., Williams, S. A., DeSilva, J. M., Skinner, M. M., Musiba, C. M., Cameron, N., Holliday, T. W., Harcourt-Smith, W., Ackermann, R. R., Bastir, M., Bogin, B., Bolter, D., Brophy, J., Cofran, Z. D., Congdon, K. A., Deane, A. S., Dembo, M., Drapeau, M., Elliott, M. C., Feuerriegel, E. M., Garcia-Martinez, D., Green, D. J., Gurtov, A., Irish, J. D., Kruger, A., Laird, M. F., Marchi, D., Meyer, M. R., Nalla, S., Negash, E. W., Orr, C. M., Radovcic, D., Schroeder, L., Scott, J. E., Throckmorton, Z., Tocheri, M. W., VanSickle, C., Walker, C. S., Wei, P., Zipfel B., 2015. *Homo naledi*, a new species of the genus *Homo* from the Dinaledi Chamber, South Africa. *eLife* 4.

Berggren, W. A., Hilgen, F. J., Langereis, C. G., Kent, D. V., Obradovich, J. D., Raffi, I., Raymo, M. E., Shackleton, N. J., 1995. Late Neogene chronology: New perspectives in high-resolution stratigraphy. *Geological Society of America Bulletin* 107, 1272-1287.

Boisserie, J.-R., Zazzo, A., Merceron, G., Blondel, C., Vignaud, P., Likius, A., Mackaye, H. T., Brunet, M., 2005. Diets of modern and late Miocene hippopotamids: evidence from carbon isotope composition and micro-wear of tooth enamel. *Palaeogeography, Palaeoclimatology, Palaeoecology* 221, 153-174.

Bradshaw, C. D., Lunt, D. J., Flecker, R., Salzmann, U., Pound, M. J., Haywood, A. M., Eronen, J. T. , 2012. The relative roles of CO_2 and palaeogeography in determining Late Miocene climate: results from a terrestrial data-model comparison. *Climate of the Past Discussions* 8, 715-786.

Brain, C. K., 1981. The hunters or the hunted? An introduction to African Cave Taphonomy. Chicago and London, The University of Chicago Press.

Broughton, P.L., 1983. Lattice Deformation and Curvature in Stalactitic Carbonate. *International Journal of Speleology* 13, 19-30.

Brunet, M., Guy, F., Pilbeam, D., Mackaye, H. T., Likius, A., Ahounta, D., Beauvilain, A., Blondel, C., Bocherens, H., Boisserie, J.-R., De Bonis, L., Coppens, Y., Dejax, J., Denys, C., Duringer, P., Eisenmann, V., Fanone, G., Fronty, P., Geraads, D., Lehmann, T., Lihoreau, F., Louchart, A., Mahamat, A., Merceron, G., Mouchelin, G., Otero, O., Campomanes, P. P., De Leon, M. P., Rage, J.-C., Sapanet, M., Schuster, M., Sudre, J., Tassy, P., Valentin, X., Vignaud, P., Viriot, L., Zazzo, A., Zollikofer, C., 2002. A new hominid from the Upper Miocene of Chad, Central Africa. *Nature* 418, 145-151.

Brunet, M., Guy, F., Pilbeam, D., Lieberman, D. E., Likius, A., Mackaye, H. T., Ponce de Leon, M. S., Zollikofer, C. P. E. and Vignaud, P., 2005. New material of the earliest hominid from the Upper Miocene of Chad. *Nature* 434, 752-755.

Cerling, T.E., Harris, J.M., MacFadden, B.J., Leakey, M.G., Quade, J., Eisenmann, V. Ehleringer, J.R., 1997. Global Vegetation Change through the Miocene-Pliocene Boundary. *Nature* 389, 153-158.

Cerling, T. E., Levin, N. E., Quade, J., Wynn, J. G., Fox, D. L., Kingston, J. D., Klein, R. G., Brown, F. H., 2010. Comment on the Paleoenvironment of *Ardipithecus ramidus. Science* 328, 1105.

Cerling, T. E., Wynn, J. G., Andanje, S. A., Bird, M. I., Korir, D. K., Levin, N. E., Mace, W., Macharia, A. N., Quade, J., Remien, C. H., 2011. Woody cover and hominin environments in the past 6 million years. *Nature* 476, 51-56.

Cheetham, A.K., 2002. Structure Determination from Powder Diffraction: An Overview. In David, W.I.F., Shankland, K., McCusker, L.B., and Baerlocher, Ch. (eds) *Structure Determination from Powder Diffraction Data.* Oxford University Press: Oxford.

Christin, P.-A., Besnard, G., Samaritani, E., Duvall, M. R., Hodkinson, T. R., Savolainen, V., Salamin, N., 2008. Oligocene CO_2 Decline Promoted C_4 Photosynthesis in Grasses. *Current Biology* 18, 37-43.

Colin, C., Siani, G., Liu, Z., Blamart, D., Skonieczny, C., Zhao, Y., Bory, A., Frank, N. Duchamp-Alphonse, S., Thil, F., Richter, T., Kissel, C. Gargani, J., 2014. Late Miocene to early Pliocene climate variability off NW Africa (ODP Site 659). *Palaeogeography, Palaeoclimatology, Palaeoecology* 401, 81-95.

Conroy, G. C., Pickford, M., Senut, B., Van Couvering, J., Mein, P., 1992. *Otavipithecus namibiensis*, first Miocene hominoid from southern Africa. *Nature* 356, 144-148.

Cruz, F. W. Jr., Burns, S. J., Karmann, I., Sharp, W. D., Vuille, M., Cardoso, A. O., Ferrari, J. A., Silva Dias, P. L., Viana, O. Jr., 2005. Insolation-driven changes in atmospheric circulation over the past 116,000 years in subtropical Brazil. *Nature* 434, 63-66.

deMenocal, P.B., 1995. Plio-Pleistocene African Climate. *Science* 270, 53-59.

Denys, C., 1999. Of mice and men: evolution in East and South Africa during Plio-Pleistocene times, *in* Bromage, T. G., and Schrenk, F., eds., African biogeography, climate change & human evolution: Oxford, Oxford University Press, p. 226-252.

Dirks, P. H. G. M., Berger, L. R., 2013. Hominin-bearing caves and landscape dynamics in the Cradle of Humankind, South Africa. *Journal of African Earth Sciences* 78, 109-131.

Dirks, P. H. G. M., Roberts, E. M., Hilbert-Wolf, H., Kramers, J. D., Hawks, J., Dosseto, A., Duval, M., Elliott, M., Evans, M., Grün, R., Hellstrom, J., Herries, A. I. R., Joannes-Boyau, R., Makhubela, T. V., Placzek, C. J., Robbins, J., Spandler, C., Wiersma, J., Woodhead, J., Berger, L. R., 2017. The age of *Homo naledi* and associated sediments in the Rising Star Cave, South Africa, eLife, 6, p. e24231.

Domínguez-Rodrigo, M., 2014. Is the "Savanna Hypothesis" a Dead Concept for Explaining the Emergence of the Earliest Hominins? *Current Anthropology* 55, 59-81.

Dupont, L. M., Rommerskirchen, F., Mollenhauer, G., Schefuß, E., 2013. Miocene to Pliocene changes in South African hydrology and vegetation in relation to the expansion of C4 plants. *Earth and Planetary Science Letters* 375, 408-417.

Dupont-Nivet, G., Hoorn, C., Konert, M., 2008. Tibetan uplift prior to the Eocene-Oligocene climate transition: Evidence from pollen analysis of the Xining Basin. *Geology* 36, 987-990.

Ehleringer, J. R., Cerling, T. E., Helliker, B. R., 1997. C-4 photosynthesis, atmospheric CO_2 and climate. *Oecologia* 112, 285-299.

Eriksson, P.G., Altermann, W., 1998. An Overview of the Geology of the Transvaal Supergroup Dolomites (South Africa). *Environmental Geology* 36, 179-188.

Fairchild, I.J., McMillan, E.A., 2007. Speleothems as Indicators of Wet and Dry Periods. *International Journal of Speleology* 36, 69-74.

Fairchild, I.J., Smith, C.L., Baker, A., Fuller, L., Spötl, C., Mattey, D., McDermott, F. and E.I.M.F., 2006. Modification and Preservation of Environmental Signals in Speleothems. *Earth-Science Reviews* 75, 105-153.

Fairchild, I.J., Treble, P.C., 2009. Trace Elements in Speleothems as Recorders of Environmental Change. *Quaternary Science Reviews* 28, 449-468.

Feakins, S. J., Levin, N. E., Liddy, H. M., Sieracki, A., Eglinton, T. I., Bonnefille, R., 2013. Northeast African vegetation change over 12 m.y. *Geology* 41, 295-298.

Flecker, R., Krijgsman, W., Capella, W., de Castro Martíns, C., Dmitrieva, E., Mayser, J. P., Marzocchi, A., Modestou, S., Ochoa, D., Simon, D., Tulbure, M., van den Berg, B., van der Schee, M., de Lange, G., Ellam, R., Govers, R., Gutjahr, M., Hilgen, F., Kouwenhoven, T., Lofi, J., Meijer, P., Sierro, F. J., Bachiri, N., Barhoun, N., Alami, A. C., Chacon, B, Flores, J. A., Gregory, J., Howard, J., Lunt, D., Ochoa, M., Pancost, R. Vincent, S., Yousfi, M. Z., 2015. Evolution of the Late Miocene Mediterranean–Atlantic gateways and their impact on regional and global environmental change. *Earth-Science Reviews* 150, 365-392.

Folk, R.L., Assereto, R., 1976. Comparative Fabrics of Length-Slow and Length-Fast Calcite and Calcitized Aragonite in a Holocene Speleothem, Carlsbad Caverns, New Mexico. *Journal of Sedimentary Petrology* 46, 486-496.

Frisia, S., Borsato, A., Fairchild, I.J., McDermott, F., Selmi, E.M., 2002. Aragonite-Calcite Relationships in Speleothems (Grotte de Clamouse, France): Environment, Fabrics, and Carbonate Geochemistry. *Journal of Sedimentary Research* 72, 687-699.

Frisia, S., Borsato, A., Fairchild, I.J., McDermott, F., 2000. Calcite Fabrics, Growth Mechanisms, and Environments of Formation in Speleothem from the Italian Alps and Southwestern Ireland. *Journal of Sedimentary Research* 70, 183-1196.

Frisia, S., 2015. Microstratigraphic logging of calcite fabrics in speleothems as tool for palaeoclimate studies. *International Journal of Speleology* 44, 1-16.

Garzione, C. N., 2008. Surface uplift of Tibet and Cenozoic global cooling. *Geology* 36, 1003-1004.

Genty, D., Massault, M., 1999. Carbon Transfer Dynamics from Bomb-^{14}C and $\delta^{13}C$ Time Series of a Laminated Stalagmite from SW France – Modelling and Comparison with other Stalagmite Records. *Geochimica et Cosmochimica Acta* 63, 1537-1548.

Genty, D., Massault, M., Gilmour, M., Baker, A., Verheyden, S., Kepens, E., 1999. Calculations of Past Dead Carbon Proportion and Variability by the Comparison of AMS ^{14}C and TIMS U/Th Ages on Two Holocene Stalagmites. *Radiocarbon* 41, 251-270.

Genty, D., Baker, A., Vokal, B., 2001. Intra- and inter-annual growth rate of modern stalagmites. Chemical Geology 176, 191-212.

Goede, A., McCulloch, M., McDermott, F., Hawkesworth, C., 1998. Aeolian Contribution to Strontium and Strontium Isotope Variations in a Tasmanian Speleothem. *Chemical Geology* 149, 37-50.

Gommery, D., Sénégas, F., Potze, S., Kgasi, L., 2014. Les primates non-humains fossiles de Bolt's Farm (Afrique du Sud). Contexte, recherches actuelles et perspectives. *BMSAP* 26, 184-189.

Granger, D. E. Gibbon, R. J., Kuman, K., Clarke, R. J., Bruxelles, L., Caffee, M. W., 2015. New cosmogenic burial ages for Sterkfontein Member 2 *Australopithecus* and Member 5 Oldowan. *Nature* 522, 85-88.

Haile-Selassie, Y., 2001. Late Miocene hominids from the Middle Awash, Ethiopia. *Nature* 412, 178-181.

Haile-Selassie, Y., Suwa, G., White, T. D., 2004. Late Miocene Teeth from Middle Awash, Ethiopia, and Early Hominid Dental Evolution. *Science* 303, 1503-1505.

Herries, A.I.R., Adams, J.W., Kuykendall, K.L., Shaw, J., 2006a. Speleology and Magnetobiostratigraphic Chronology of the GD 2 Locality of the Gondolin Hominin-Bearing Paleocave Deposits, North West Province, South Africa. *Journal of Human Evolution* 51, 617-631.

Herries, A.I.R., Reed, K.E., Kuykendall, K.L., Latham, A.G., 2006b. Speleology and magnetobiostratigraphic Chronoloy of the Buffalo Cave Fossil Site, Makapansgat, South Africa. *Quaternary Research* 66, 233-245.

Herries, A. I. R., Curnoe, D., Adams, J. W., 2009. A multi-disciplinary seriation of early *Homo* and *Paranthropus* bearing palaeocaves in southern Africa. *Quaternary International* 202, 14-28.

Herries, A. I. R., Shaw, J., 2011. Palaeomagnetic analysis of the Sterkfontein palaeocave deposits: Implications for the age of the hominin fossils and stone tool industries. *Journal of Human Evolution* 60, 523-539.

Herries, A. I. R., Adams, J. W., 2013. Clarifying the context, dating and age range of the Gondolin hominins and *Paranthropus* in South Africa. *Journal of Human Evolution* 65, 676-681.

Hill, C. A., Forti, P., 1997. *Cave Minerals of the World*. National Speleological Society, Huntsville, Alabama, pp. 462.

Hoetzel, S., Dupont, L., Schefuβ, E., Rommerskirchen, F., Wefer, G., 2013. The role of fire in Miocene to Pliocene C4 grassland and ecosystem evolution. *Nature Geoscience* 6, 1027-1030.

Hoetzel, S., Dupont, L. M., Wefer G., 2015. Miocene–Pliocene vegetation change in south-western Africa (ODP Site 1081, offshore Namibia). *Palaeogeography, Palaeoclimatology, Palaeoecology* 423, 102-108.

Holmgren, K., Lee-Thorp, J. A., Cooper, G. R. J., Lundblad, K., Partridge, T. C., Scott, L., Sithaldeen, R., Talma, A. T, Tyson, P. D., 2003. Persistent Millennial-Scale Climatic Variability over the past 25000 Years in Southern Africa. *Quaternary Science Reviews* 22, 2311-2326.

Holzkämper, S., Holmgren, K., Lee-Thorp, J., Talma, S., Mangini, A., Partridge, T., 2009. Late Pleistocene Stalagmite Growth in Wolkberg Cave, South Africa. *Earth and Planetary Science Letters* 282, 212-221.

Hopley, P. J., Latham, A. G., Marshall, J. D., 2006. Palaeoenvironments and palaeodiets of mid-Pliocene micromammals from Makapansgat Limeworks, South Africa: a stable isotope and dental microwear approach: *Palaeogeography, Palaeoclimatology, Palaeoecology* 233, 235-251.

Hopley, P.J., Marshall, J.D., Weedon, G.P., Latham, A.G., Herries, A.I.R., Kuykendall, K.L., 2007a. Orbital Forcing and the Spread of C4 Grasses in the Late Neogene: Stabe Isotope Evidence from South African Speleothems. *Journal of Human Evolution* 53, 620-634.

Hopley, P.J., Weedon, G.P., Marshall, J.D., Herries, A.I.R., Latham, A.G., and Kuykendall, K.L., 2007b. High- and Low-Latitude Orbital Forcing of Early Hominin Habitats in South Africa. *Earth and Planetary Science Letters* 256, 419-432.

Hopley, P.J., Marshall, J.D., Latham, A.G., 2009. Speleothem Preservation and Diagenesis in South African Hominin Sites: Implication for Palaeoenvironments and Geochronology. *Geoarchaeology* 24, 519-547.

Hopley, P. J., Maslin, M. A., 2010. Climate-averaging of terrestrial faunas: an example from the Plio-Pleistocene of South Africa. *Paleobiology* 36, 32-50.

Hopley, P. J., Weedon, G. P., Brierley, C. M., Thrasivoulou, C., Herries, A. I. R., Dinckal, A., Richards, D. A., Nita, D. C., Parrish, R. R., Roberts, N. M. W., Sahy, D., Smith, C. L., 2018. Orbital precession modulates interannual rainfall variability, as recorded in an Early Pleistocene speleothem. *Geology* 46, 731-734.

Hopley, P. J. (in press). Environmental, stratigraphic and taxonomic bias in the hominin fossil record: implications for theories of the climatic forcing of human evolution. In, African Palaeoenvironments (Eds, Reynolds, S. C. and Bobe, R.).

Huang, Y., Fairchild, I.J., 2001. Partitioning of Sr^{2+} and Mg^{2+} into Calcite under Karst-Analogue Experimental Conditions. *Geochimica et Cosmochimica Acta* 65, 47-62.

Ivanovic, R. F., Valdes, P. J., Flecker, R., Gutjahr, M., 2014. Modelling global-scale climate impacts of the late Miocene Messinian Salinity Crisis. *Clim. Past* 10, 607-622.

Jones, C. H., 2002. User-driven integrated software lives: 'Paleomag' Paleomagnetic analysis on the Macintosh TM. *Computers and Geosciences* 28, 1145-51.

Kingston, J. D., 2007. Shifting adaptive landscapes: Progress and challenges in reconstructing early hominid environments. *Yearbook of Physical Anthropology* 134, 20-58.

Kirschvink, J. L., 1980. The least-squares line and plane and the analysis of palaeomagnetic data. *Geophysical Jounral of the Royal Astronomical Society* 62, 699-718.

Kirschvink, J. L., Kopp, R. E., Raub, T. D., Baumgartner, C. T., Holt, J. W., 2008. Rapid, precise, and high-sensitivity acquisition of paleomagnetic and rock-magentic data: Development of a low-noise

automatic sample changing system for superconducting rock magnetometers. *Geochemistry, Geophysics and Geosystems* 9: Q05Y01, doi: 10.1029/2007GC001856.

Kramers, J. D., Dirks, P. H. G. M., 2017. The age of fossil StW573 ('Little Foot'): An alternative interpretation of $^{26}Al/^{10}Be$ burial data. *South African Journal of Science* 113, 2016-0085.

Krijgsman, W., Hilgen, F. J., Raffi, I., Sierro, F. J., Wilson, D. S., 1999. Chronology, causes and progression of the Messinian salinity crisis. *Nature* 400, 652-655.

Krijgsman, W., Fortuin, A. R., Hilgen, F. J., Sierro, F. J., 2001. Astrochronology for the Messinian Sorbas basin (SE Spain) and orbital (precessional) forcing for evaporite cyclicity. *Sedimentary Geology* 140, 43-60.

Kronfeld, J., Vogel, J. C., Talma, A. S., 1994. A new explanation for extreme $^{234}U/^{238}U$ disequilibria in a dolomitic aquifer. *Earth and Planetary Science Letters* 123, 81-93.

Kürschner, W. M., Kvaček, Z.., Dilcher, D. L, 2008. The impact of Miocene atmospheric carbon dioxide fluctuations on climate and the evolution of terrestrial ecosystems. *Proceedings of the National Academy of Sciences* 105, 449-453.

Langergraber, K. E., Prüfer, K., Rowney, C., Boesch, C., Crockford, C., Fawcett, K., Inoue, E., Inoue-Muruyama, M., Mitani, J. C., Muller, M. N., Robbins, M. M., Schubert, G., Stoinski, T. S., Viola, B., Watts, D., Wittig, R. M., Wrangham, R. W., Zuberbühler, K., Pääbo, S., Vigilant, L., 2012. Generation times in wild chimpanzees and gorillas suggest earlier divergence times in great ape and human evolution. *Proceedings of the National Academy of Sciences* 109, 15716-15721.

Lachniet, M.S., 2009. Climatic and Environmental Controls on Speleothem Oxygen-Isotope Values. *Quaternary Science Reviews* 28, 412-432.

Lebatard, A.-E., Bourles, D. L., Duringer, P., Jolivet, M., Braucher, R., Carcaillet, J., Schuster, M., Arnaud, N., Monie, P., Lihoreau, F., Likius, A., Mackaye, H. T., Vignaud, P., Brunet, M. (2008). Cosmogenic nuclide dating of Sahelanthropus tchadensis and Australopithecus bahrelghazali: Mio-Pliocene hominids from Chad. *Proceedings of the National Academy of Sciences of the United States of America* 105, 3226-3231.

Lee-Thorp, J.A., Sponheimer, M., and Luyt, J., 2007. Tracking Changing Environments using Stable Carbon Isotopes in Fossil Tooth Enamel: An Example from the South African Hominin Sites. *Journal of Human Evolution* 53, 595-601.

Levin, N. E., 2013. Compilation of East Africa Soil Carbonate Stable Isotope Data. *EarthChem Library*. http://dx.doi.org/10.1594/IEDA/100231.

Levin, N. E., 2015. Environment and Climate of Early Human Evolution. *Annual Review of Earth and Planetary Sciences* 43: 405-429.

Lüdecke, T. Schrenk, F., Thiemeyer, H., Kullmer, O., Bromage, T. G., Sandrock, O., Fiebig, J., Mulch, A., 2016. Persistent C3 vegetation accompanied Plio-Pleistocene hominin evolution in the Malawi Rift (Chiwondo Beds, Malawi). *Journal of Human Evolution* 90, 163-175.

Manzi, V., Gennari, R., Hilgen, F., Krijgsman, W., Lugli, S., Roveri, M., Sierro F. J., 2013. Age refinement of the Messinian salinity crisis onset in the Mediterranean. *Terra Nova* 25, 315-322.

Marshall, C. R., 1990. Confidence-intervals on stratigraphic ranges. *Paleobiology* 16, 1-10.

McDermott, F., 2004. Palaeo-Climate Reconstructions from Stable Isotope Variations in Speleothems: A Review. *Quaternary Science Reviews* 23, 901-918.

McKee, J. K., Thackeray, J. F., Berger, L. R., 1995. Faunal assemblage seriation of southern African Pliocene and Pleistocene fossil deposits. *American Journal of Physical Anthropology* 96, 235-250.

Mickler, P. J., Stern, L. A., Banner, J. L., 2006. Large kinetic isotope effects in modern speleothems: Geological Society of America Bulletin 118, 65-81.

Morgan, M. E., Kingston, J. D., Marino, B. D., 1994. Carbon isotopic evidence for the emergence of C4 plants in the Neogene from Pakistan and Kenya: *Nature* 367, 162-165.

Ogg, J. G., 2012. Geomagnetic Polarity Time Scale, *in* Gradstein, F. M., Ogg, J. G., Schmitz, M. D., and Ogg, G. M., eds., The Geologic Time Scale, Elsevier, p. 85-113.

Osborne, C., 2007. Atmosphere, ecology and evolution: what drove the Miocene expansion of C-4 grasslands? *Journal of ecology* 96, 35-45.

Otero, O. Lécuyer, C., Fourel, F., Martineau, F., Mackaye, H. T., Vignaud, P., Brunet, M., 2011. Freshwater fish $\delta^{18}O$ indicates a Messinian change of the precipitation regime in Central Africa. *Geology* 39, 435-438.

Pagani, M., Freeman K. H., Arthur M. A., 1999. Late Miocene atmospheric CO_2 concentrations and the expansion of C4 grasses. *Science* 285, 876-879.

Partridge, T. C., 2010. Tectonics and Geomorphology of Africa during the Phanerozoic. In, Cenozoic Mammals of Africa (edited by Werdelin, L.). University of California Press pp. 3-18.

Pickering, R., Hancox, P.J., Lee-Thorp, J.A., Grün, Mortimer, G.A., McCulloch, M., and Berger, L.R., 2007. Stratigraphy, U-Th Chronology, and Paleoenvironments at Gladysvale Cave: Insight into the Climatic Control of South African Hominin-Bearing Cave Deposits. *Journal of Human Evolution* 53, 602-619.

Pickering, R., Dirks, P. H. G. M., Jinnah, Z., de Ruiter, D. J., Churchill, S. E., Herries, A. I. R., Woodhead, J. D., Hellstrom, J. C., Berger, L. R., 2011. *Australopithecus sediba* at 1.977 Ma and implications for the origins of the genus *Homo*. *Science* 333, 1421-1423.

Pickford, M., Senut, B., 2001. The geological and faunal context of Late Miocene hominid remains from Lukeino, Kenya. *Comptes Rendus De L Academie Des Sciences Serie Ii Fascicule a- Sciences de la Terre et des Planetes* 332, 145-152.

Pickford, M., 2004. Southern Africa: a cradle of evolution. *South African Journal of Science* 100, 205-214.

Pocock, T. N., 1976. Pliocene mammalian microfauna from Langebaanweg: A new fossil genus linking the Otomyinae with the Murinae. *South African Journal of Science* 72, 58-60.

Polyak, V., Hill, C., Asmerom, Y., 2008. Age and evolution of the Grand Canyon revealed by U-Pb dating of water table-type speleothems. *Science* 319, 1377-1380.

Renne, P. R., Wolde-Gabriel, G., Hart, W. K., Heiken, G. White, T. D., 1999. Chronostratigraphy of the Miocene-Pliocene Sagantole Formation, Middle Awash Valley, Afar rift, Ethiopia. *Geological Society of America Bulletin* 111, 869-885.

Reynolds, S. C., Kibii, J. M., 2011. Sterkfontein at 75: review of palaeoenvironments, fauna and archaeology from the hominin site of Sterkfontein (Gauteng Province, South Africa). *South African Journal of Science* 46, 59-88.

Reynolds, S. C., Bailey, G. N., King, G. C. P., 2011. Landscapes and their relation to hominin habitats: Case studies from *Australopithecus* sites in eastern and southern Africa. *Journal of Human Evolution* 60, 281-298.

Roberts, N. M. W., Rasbury, E. T., Parrish, R. R., Smith, C. J., Horstwood, M. S.A., Condon, D. J., 2017. A calcite reference material for LA-ICP-MS U-Pb geochronology. *Geochemistry, Geophysics, Geosystems*. 10.1002/2016GC006784

Roche, D., Segalen, L., Senut, B., Pickford, M., 2013. Stable isotope analyses of tooth enamel carbonate of large herbivores from the Tugen Hills deposits: Palaeoenvironmental context of the earliest Kenyan hominids. *Earth and Planetary Science Letters* 381, 39-51.

Romanek, C.S., Grossman, E.L., Morse, J.W., 1992. Carbon Isotopic Fractionation in Synthetic Aragonite and Calcite: Effects of Temperature and Precipitation Rate. *Geochimica et Cosmochimica Acta,* 56, 419-430.

Scheiter, S., Higgins, S. I., Osborne, C. P., Bradshaw, C., Lunt, D., Ripley, B. S., Taylor, L. L., Beerling, D. J., 2012. Fire and fire-adapted vegetation promoted C4 expansion in the late Miocene. *New Phytologist* 195, 653-666.

Schneck, R., Micheels, A., Mosbrugger, V., 2010. Climate modelling sensitivity experiments for the Messinian Salinity Crisis. Palaeogeography, Palaeoclimatology, Palaeoecology 286, 149-163.

Ségalen, L., Renard, M., Lee-Thorp, J. A., Emmanuel, L., Le Callonnec, L., de Rafelis, M., Senut, B., Pickford, M., Melice J.-L., 2006. Neogene climate change and emergence of C4 grasses in the Namib, southwestern Africa, as reflected in ratite ^{13}C and ^{18}O. *Earth and Planetary Science Letters* 244, 725-734.

Ségalen, L., Lee-Thorp, J.A., Cerling, T., 2007. Timing of C4 grass expansion across Sub-Saharan Africa. *Journal of Human Evolution* 53, 549-559.

Senut, B., Pickford, M., Mein, P., Conroy, G., Van Couvering, J., 1992. Discovery of 12 new Late Cainozoic fossiliferous sites in palaeokarsts of the Otavi Mountains, Namibia. *Comptes Rendus de L'Academie des Sciences Serie II* 314, 727-733.

Senut, B., Gommery, D., 1997. Postcranial skeleton of *Otavipithecus*, Hominoidea from the Middle Miocene of Namibia. *Annales de Paleontologie* 83, 267-284.

Senut, B., Pickford, M., Gommery, D., Mein, P., Cheboi, K., Coppens, Y., 2001. First hominid from the Miocene (Lukeino Formation, Kenya). *Comptes Rendus de L'Academie des Sciences Serie Ii Fascicule A- Sciences de la Terre et des Planetes* 332, 137-144.

Sepulchre, P., Ramstein, G., Fluteau, F., Schuster, M., Tiercelin, J.-J., Brunet M., 2006. Tectonic Uplift and Eastern Africa Aridification. *Science* 313, 1419-1423.

Simpson, S. W., Kleinsasser, L., Quade, J., Levin, N. E., McIntosh, W. C., Dunbar, N., Semaw, S., Rogers, M. J., 2015. Late Miocene hominin teeth from the Gona Paleoanthropological Research Project area, Afar, Ethiopia. *Journal of Human Evolution* 81, 68-82.

Sutton, M. B., Pickering, T. R., Pickering, R., Brain, C. K., Clarke, R. J., Heaton, J. L., Kuman, K., 2009. Newly discovered fossil- and artifact-bearing deposits, uranium-series ages, and Plio-Pleistocene hominids at Swartkrans Cave, South Africa. *Journal of Human Evolution* 57, 688-696.

Veizer, J., Clayton, R.N., and Hinton, R.W., 1992. Geochemistry of Precambrian Carbonates: IV. Early Paleoproterozoic (2.25 ± 0.25 Ga) Seawater. *Geochimica et Cosmochimica Acta* 56, 857-885.

Walker, J., Cliff, R. A., Latham, A. G., 2006. U-Pb Isotopic Age of the StW 573 Hominid from Sterkfontein, South Africa. *Science* 314, 1592-1594.

White, T. D., Ambrose, S. H., Suwa, G., Su, D. F., DeGusta, D., Bernor, R. L., Boisserie, J.-R., Brunet, M., Delson, E., Frost, S., Garcia, N., Giaourtsakis, I. X., Haile-Selassie, Y., Howell, F. C., Lehmann, T., Likius, A., Pehlevan, C., Saegusa, H., Semprebon, G., Teaford, M., Vrba, E., 2009. Macrovertebrate Paleontology and the Pliocene Habitat of *Ardipithecus ramidus*. *Science* 326, 67-93.

Woodhead, J. D., Sniderman, J. M. K. , Hellstrom, J., Drysdale, R. N., Maas, R., White, N., White, S. Devine, P., 2019. The antiquity of Nullarbor speleothems and implications for karst palaeoclimate archives. *Scientific Reports* 9, 603.

Zachos, J., Pagani, M., Sloan, L., Thomas, E., and Billups, K., 2001. Trends, Rhythms, and Aberrations in Global Climate 65 Ma to Present. *Science* 292, 686-693.

Zhang, Y. G., Pagani, M., Liu, Z., Bohaty, S. M., and DeConto, R., 2013. A 40-million-year history of atmospheric CO_2: *Philosophical Transactions of the Royal Society of London A: Mathematical, Physical and Engineering Sciences* 371, no. 2001.

Zhang, Z., Ramstein, G., Schuster, M., Li, C., Contoux C., Yan, Q., 2014. Aridification of the Sahara desert caused by Tethys Sea shrinkage during the Late Miocene. *Nature* 513, 401-404.

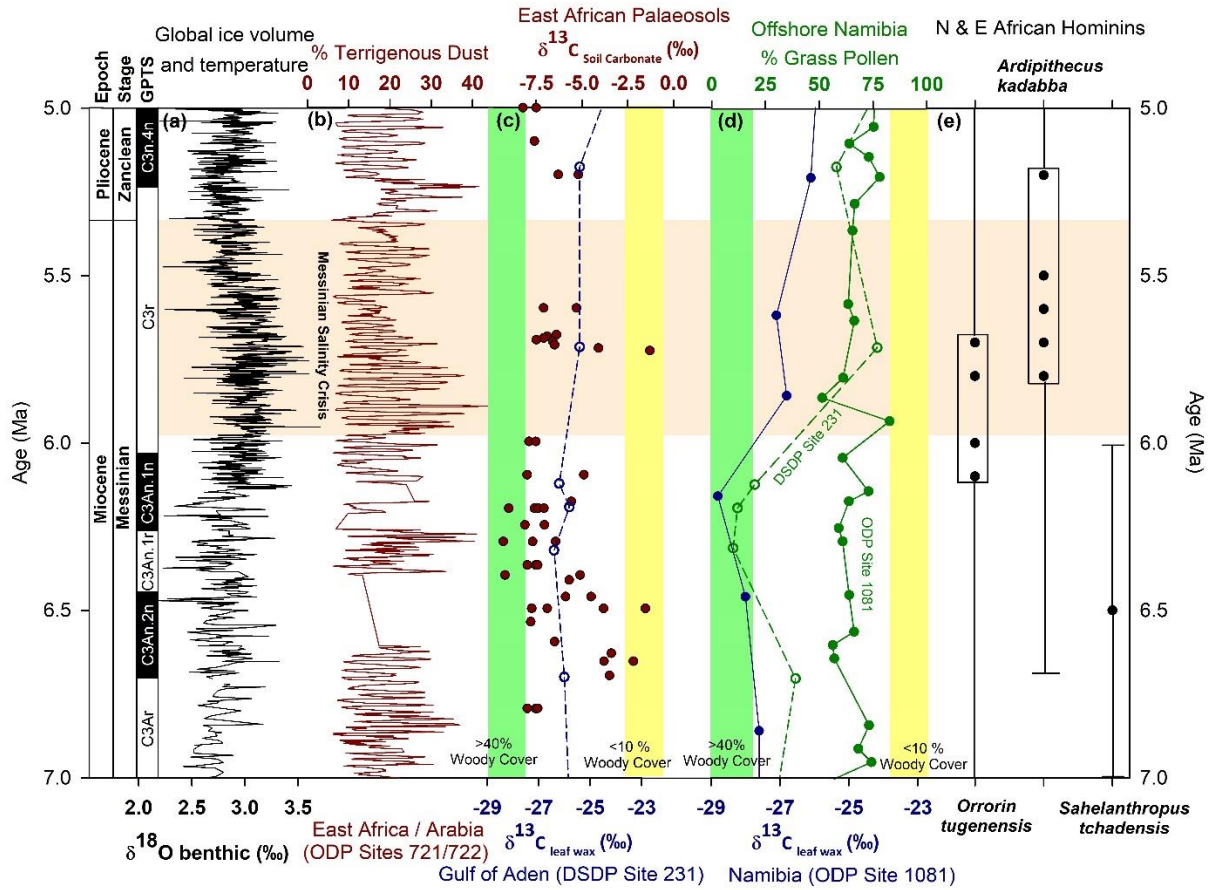

Figure 1. Compilation of data relevant to Late Miocene (Messinian) climate change and early hominin evolution in Africa. The Global Polarity Timescale (GPTS) for the Messinian is based on Krijgsmann et al. (2001). (a) The benthic foraminifera data from a global compilation by Zachos et al. (2001) represents polar ice volume and global temperatures; an increase in $\delta^{18}O$ values occurs during the Messinian Salinity Crisis, MSC (5.97 Ma to 5.33 Ma; light-brown shading). (b) The Arabian Sea dust record (ODP Sites 721 and 722) represents dust supply from the Sahara, northeast Africa and Arabia (deMenocal, 1995) shows an increase during the early MSC. (c) East African palaeosol $\delta^{13}C$ data (Levin, 2013; Levin, 2015) is a proxy for the percentage of woody cover; green shading represents >40% woody cover (closed woodland); yellow shading represents <10% woody cover (C_4 grassland; Cerling et al., 2011). East African Leaf wax $\delta^{13}C$ and grass pollen percentage (d) from the Gulf of Aden, DSDP Site 231 (Feakins et al., 2013) shows invariant Messinian carbon isotope values (i.e. no change in the proportion of C_4 plants) but an increase in the proportion of grass pollen around the onset of the MSC. In southern Africa, at ODP Site 1081, off the west coast of Namibia (d), the percentage of grass pollen is static, whereas an increase in carbon isotope values (i.e. increase proportion of C_4 plants) is observed at this time (Hoetzel et al., 2013). (e) Stratigraphic ranges for the three Miocene hominin species. Black circles represent the individual stratigraphic horizons from which each species has been recovered (Hopley, in press) and are used to calculate the 95% confidence intervals on the stratigraphic ranges, following Marshall (1990). *Sahelanthropus tchadensis* is identified from just one stratigraphic horizon, so the error bars represent the age uncertainty for this locality (Lebatard et al., 2008).

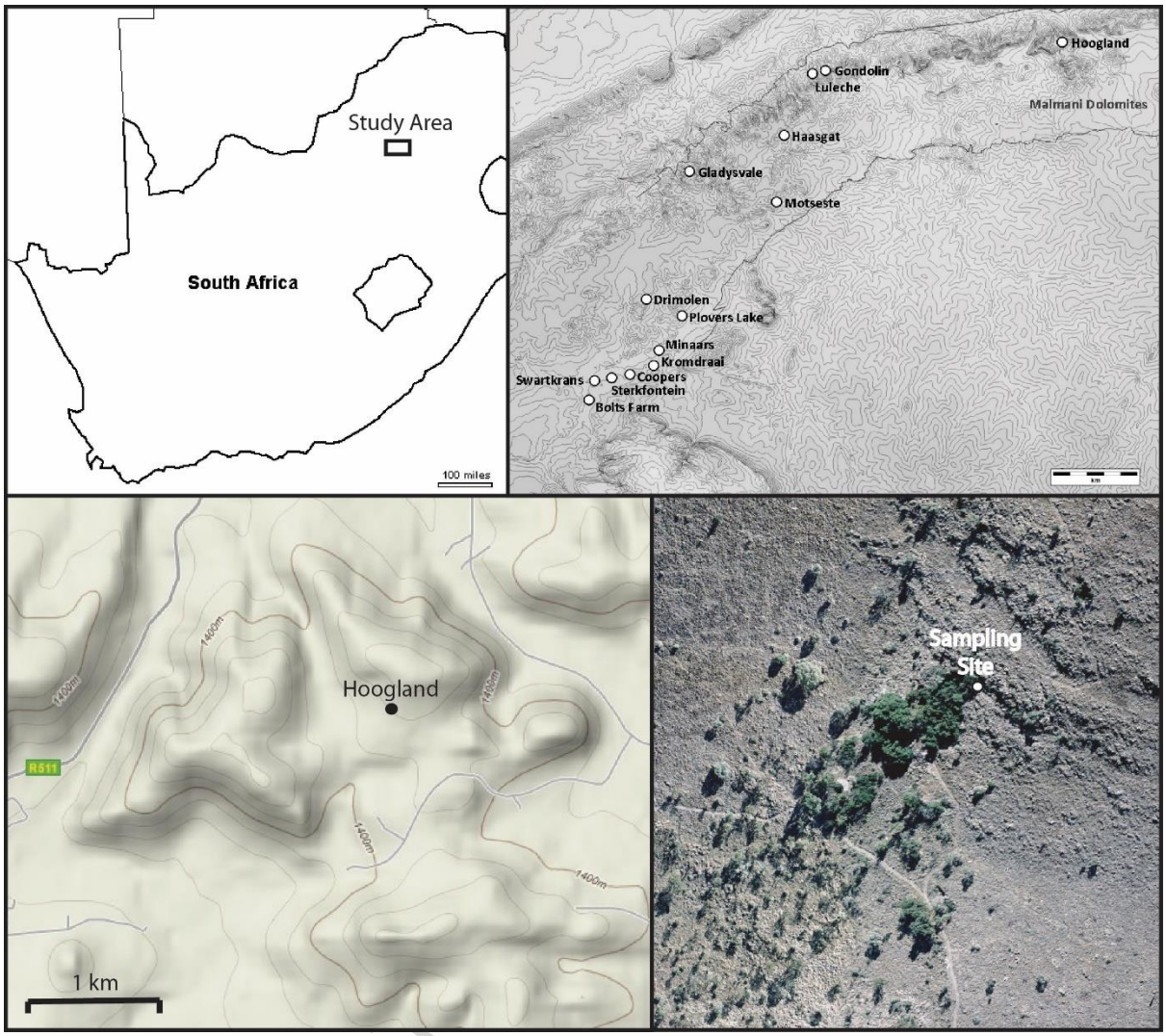

Figure 2. Location of the Hoogland cave system, showing from left to right, top to bottom: the location of Hoogland in South Africa, its location in relation to the other cave systems of the area, the topography of the local area, and an aerial photograph of the site.

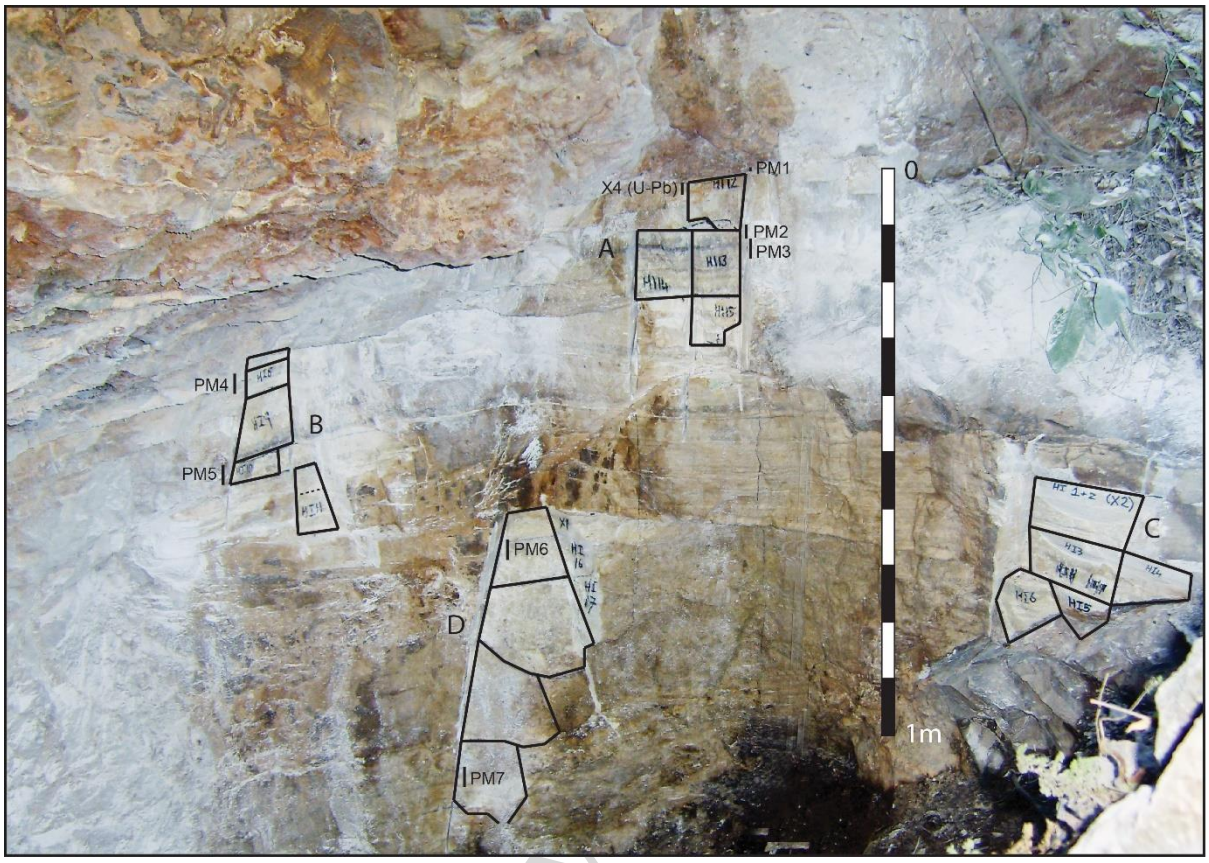

Figure 3. Sample locations of the four sections taken to cover the complete sequence of the Hoogland Southern Basal Speleothem (from top to bottom A-D).

Figure 4. Stratigraphy of the Hoogland Southern Basal Speleothem. From left to right: scale bar in 10 cm intervals; cut and polished rock sections; speleothem stratigraphic diagram based on visual assessment with corresponding low magnification thin sections; simplified stratigraphic diagram, distinguishing layers of primary aragonite, primary calcite, and secondary calcite. Location of polished sections A-D can be seen in Figure 3; high-magnification images of thin sections 1-5 are shown in Figure 5. PM indicates palaeomagnetism samples; X4 indicates sample used for uranium-lead dating.

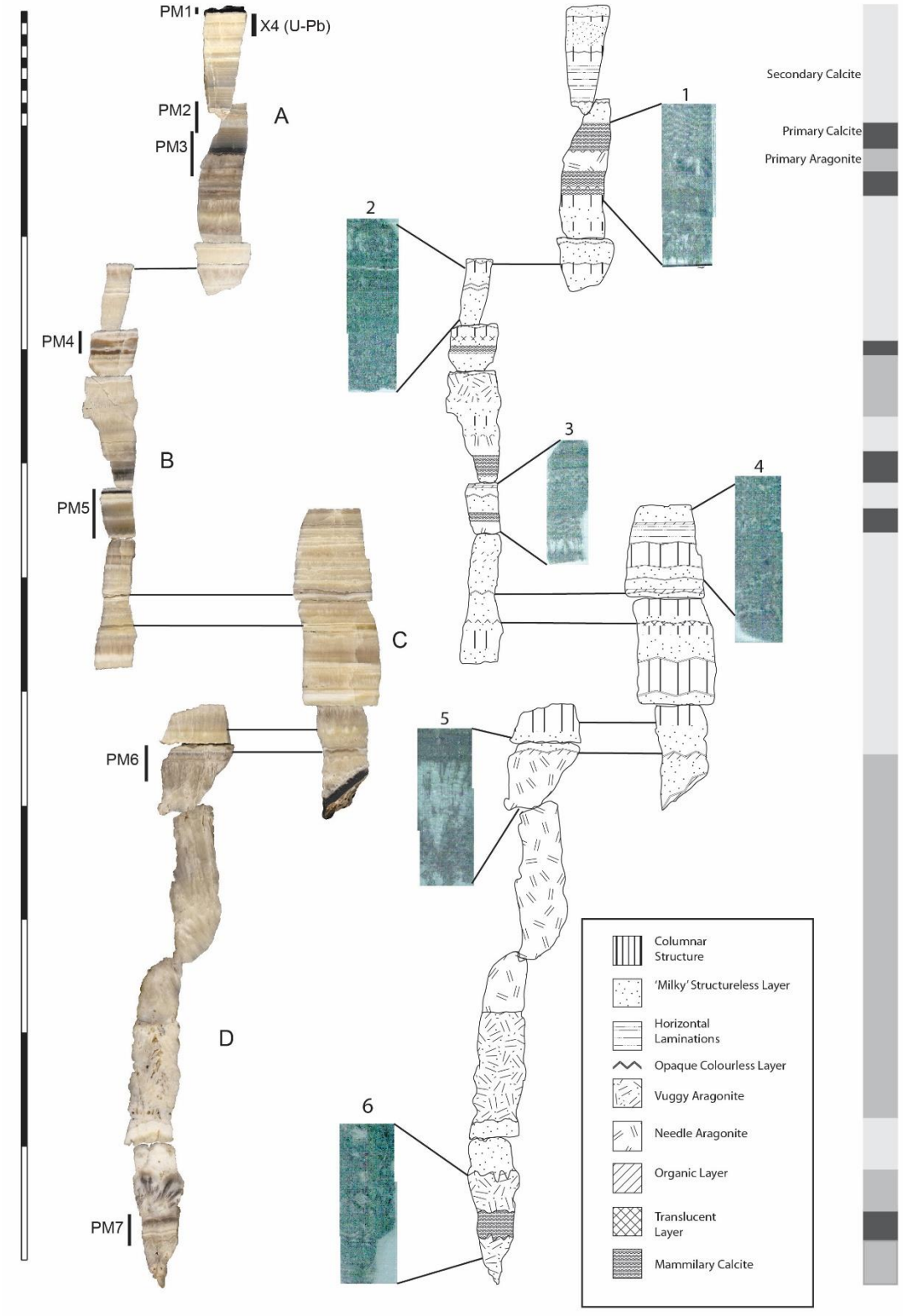

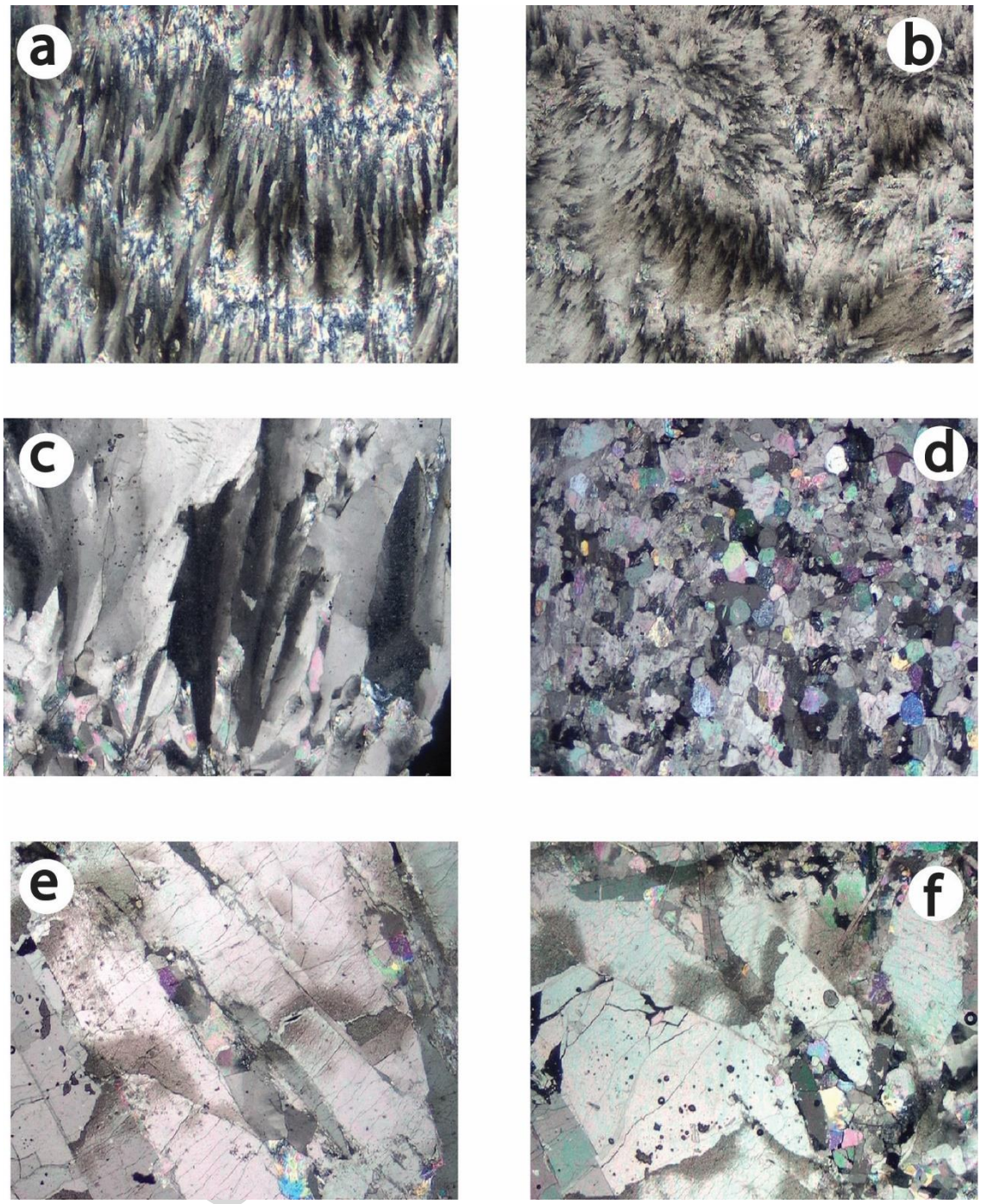

Figure 5. Photomicrographs of the Hoogland Southern Basal Speleothem in thin section. Representative fabrics include: (a, b) lattice deformed mammillary calcite (thin sections 1 and 6 respectively); (c) columnar (radiaxial fibrous) calcite (thin section 3); (d) mosaic calcite (thin section 2); (e) primary aragonite (thin sections 5) crystals; (f) aragonite with mosaic calcite, indicative of minor recrystallization (thin section 1). The location of each thin section within the speleothem sequence is shown in Figure 4. Speleothem fabric terminology from Frisia (2015) and Broughton (1983). All images taken under crossed polars; width of each field of view is 4.4 mm.

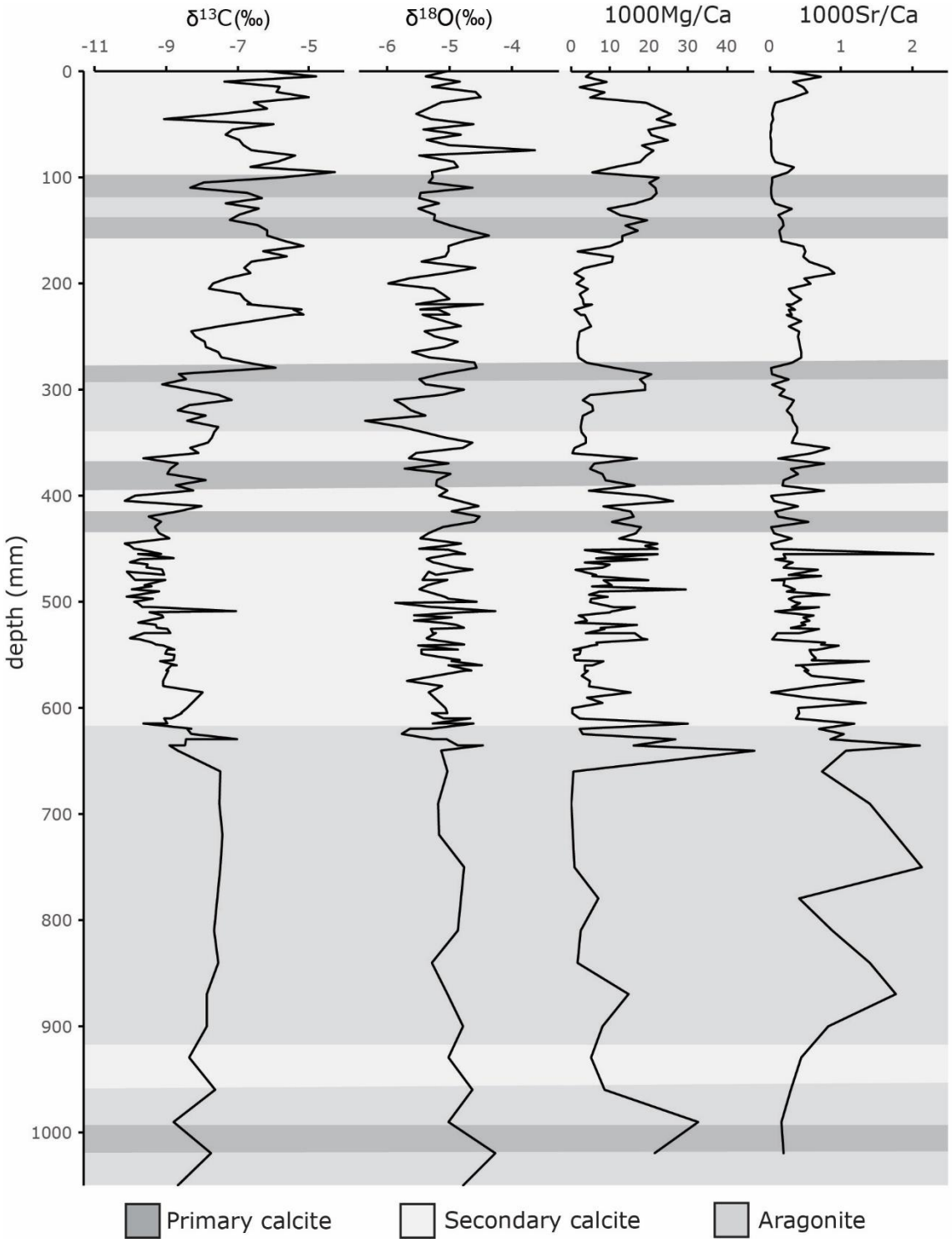

Figure 6. 1000Mg/Ca, 1000Sr/Ca, $\delta^{18}O$ and $\delta^{13}C$ ratios plotted against depth. Shaded sections indicate (from dark to light) primary calcite, aragonite, and secondary calcite. Every sample was assigned to one of these 3 categories based upon a combined interpretation of XRD results and thin section and visual assessment.

Figure 7. Four uncorrected U-Pb isochron ages for speleothem sample Hoogland X4. (a) uncorrected LA-MC-ICP-MS $^{238}U/^{206}Pb$ age, (b) uncorrected TIMS isotope dilution $^{238}U/^{206}Pb$ isochron, (c) uncorrected TIMS isotope dilution $^{238}U/^{204}Pb$ isochron, (d) TIMS isotope dilution $^{235}U/^{207}Pb$ isochron age. All uncorrected ages show close agreement. See text and Supplementary Tables S3 and S6 for discussion of measured [U] and assumptions of initial [U] used in the calculation of the corrected age.

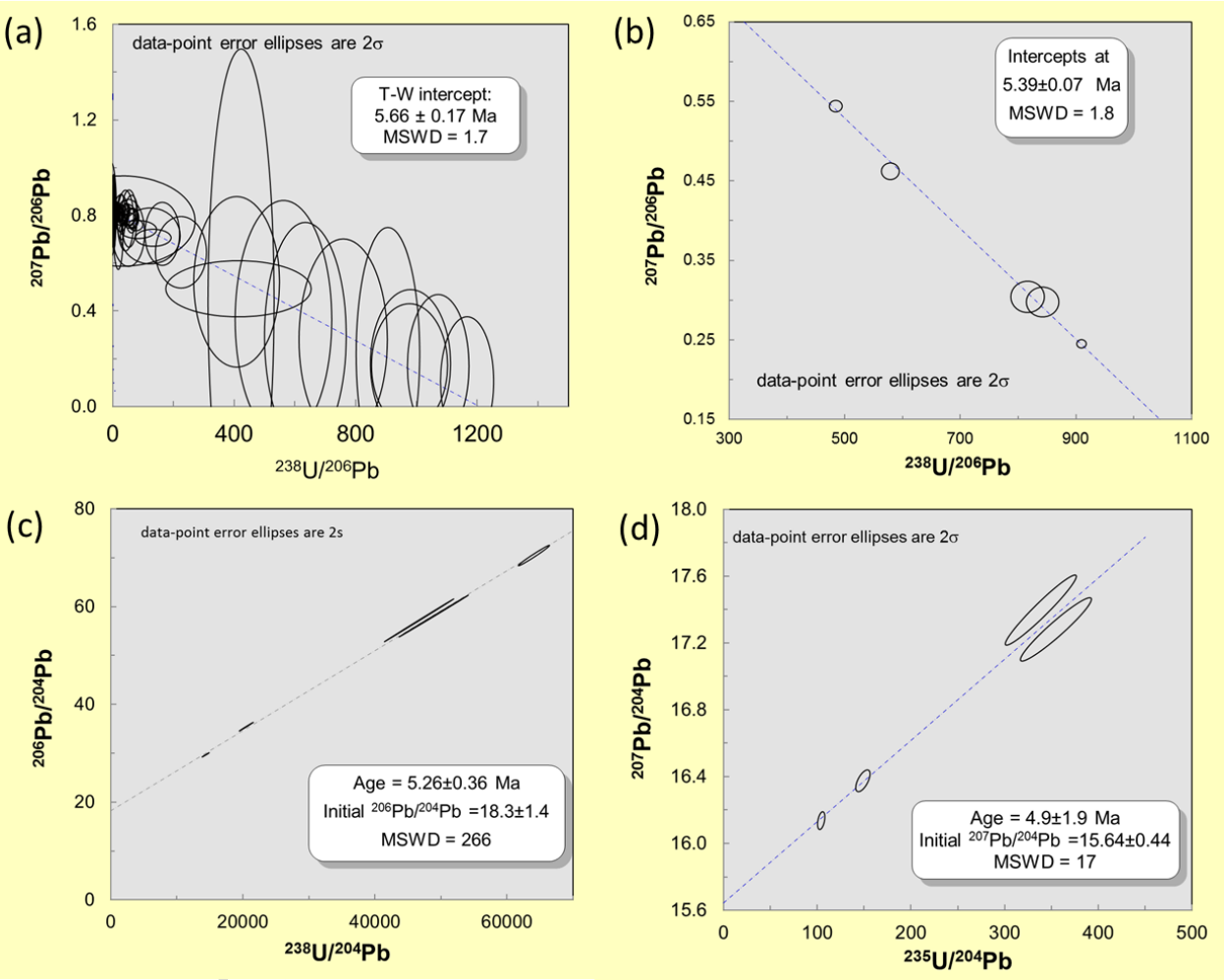

Figure 8. Representative demagnetization behavior of the Southern Basal Speleothem plotted on equal area projection. (a) Sample PM1 displays southwesterly downward directed (reversed) magnetization after removal of a lower stability magnetic component. (b) Weaker magnetized sample PM3, (c) PM5, and PM6 (not shown) also show southwesterly downward directed (reversed) magnetizations at high temperature demagnetization steps. (d) Sample PM4, and PM7 (not shown), are magnetized in a northeasterly and upward direction (normal).

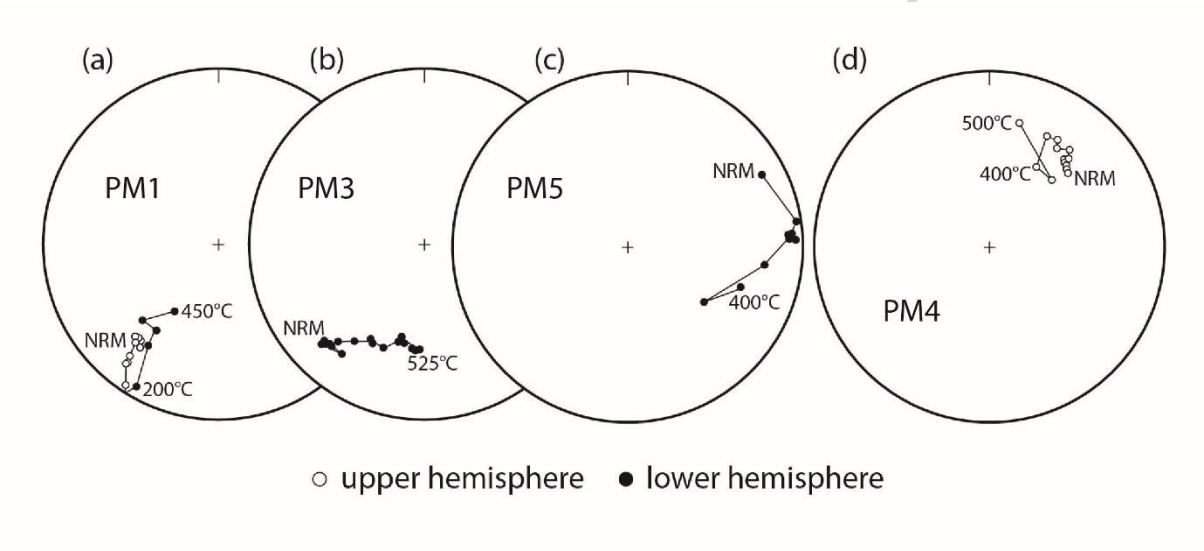

Figure 9. Magnetostratigraphy and age of the Hoogland Southern Basal Speleothem (SBS). The top of the Southern Basal Speleothem (SBS) and has a reversed polarity and a corrected uranium-lead age (Hoogland X4) of 5.28 ± 0.12 Ma; other U-Pb evidence, including alternative corrections place this sample within a broader time range of 5.8 Ma to 4.8 Ma, as indicated by the dashed line. The lower layers of the speleothem have reversed and normal polarities and are late Messinian (Late Miocene) in age (C3r Chron; Ogg et al., 2012) under all plausible dating scenarios. Stratigraphic terminology from Adams et al. (2010).

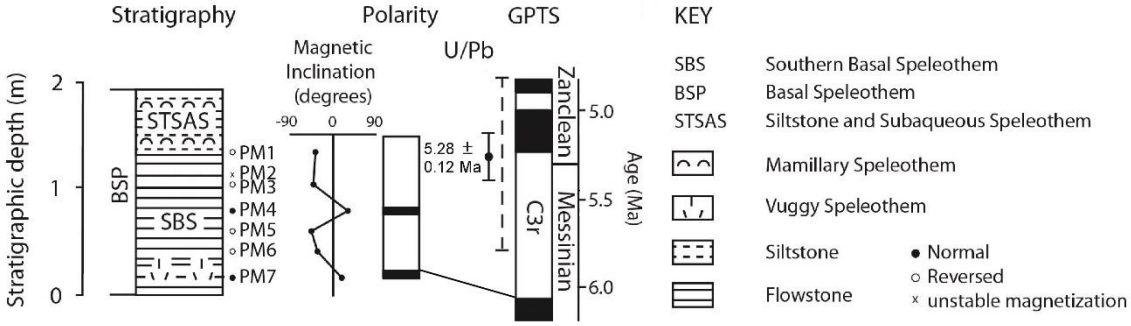

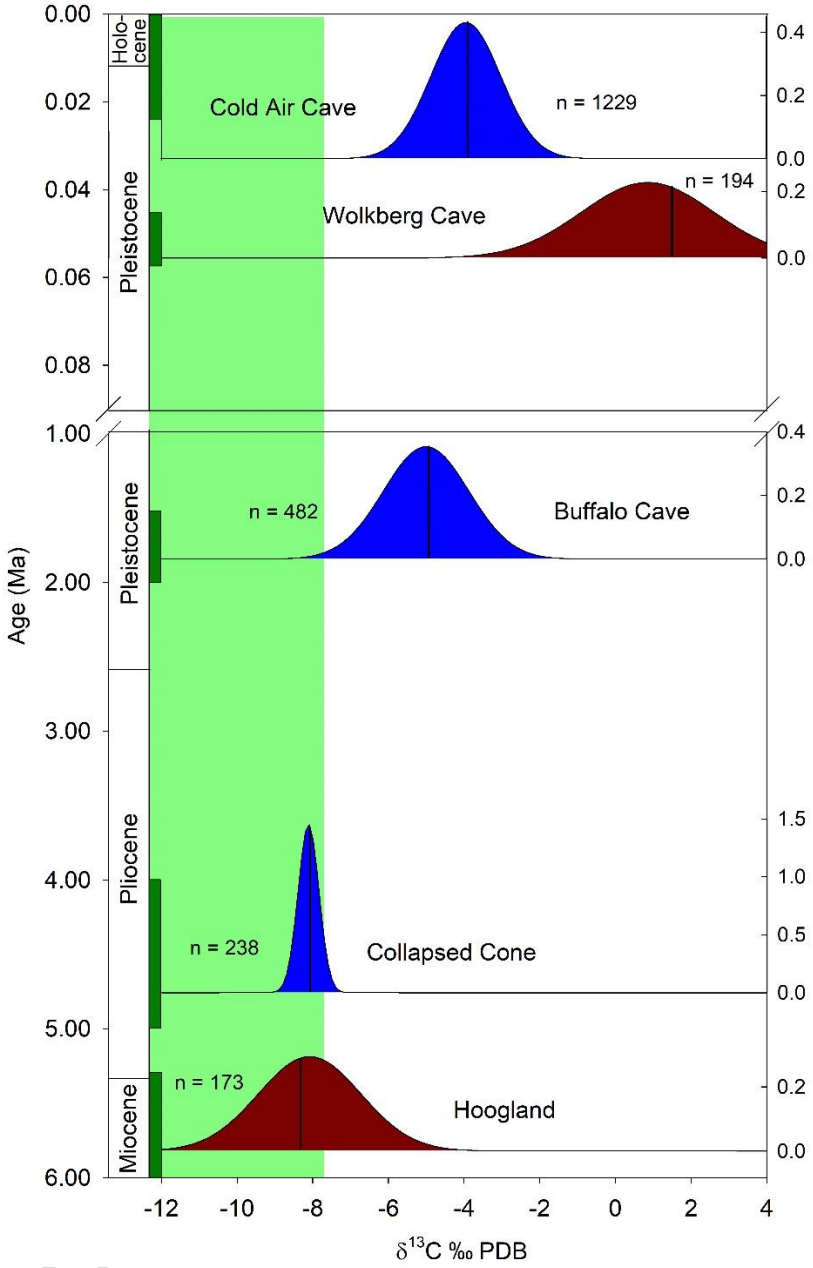

Figure 10. A compilation of carbon isotope data from Miocene to Recent speleothems from South Africa. Data is presented as normalised probability density distributions; the number of carbon isotope measurements (n) for each speleothem is indicated, along with the median value (thick black line). The dark green bars indicate the time span of each speleothem, based on U-Th dating (Cold Air Cave and Wolkberg Cave), orbital tuning and magnetostratigraphy (Buffalo Cave) and U-Pb dating (this study); the dark green bars for the Collapsed Cone flowstone and Hoogland Southern Basal Speleothem represents dating uncertainty, rather than the duration of speleothem growth. Blue shading indicates primary speleothem fabrics; red shading indicates secondary speleothem fabrics. Light green shading indicates a purely C_3 vegetation. Data from Holmgren et al. (2003); Hopley et al. (2007a,b) and Holzkamper et al. (2009).

Highlights

- Speleothem from South Africa dated to late Messinian age, using U-Pb methods
- Carbon isotopes indicate a predominantly C_3 vegetation at this time
- First savannah grasslands in southern Africa occur later than in eastern Africa
- Implications for early hominin environments